AFCRL-63-575

# PROMPT ACTIVATION ANALYSIS FOR BORON AND LITHIUM

Lincoln Clark, Jr.
Norman C. Rasmussen

Massachusetts Institute of Technology
77 Massachusetts Avenue
Cambridge, Massachusetts

Scientific Report No. 2

MITNE-42

Contract No. AF19(604)-7492

Project 4608
Task 460801

October 1963

Prepared for

Air Force Cambridge Research Laboratories
Office of Aerospace Research
United States Air Force
Bedford, Massachusetts

Requests for additional copies by Agencies of the Department of Defense, their contractors, and other Government agencies should be directed to the:

DEFENSE DOCUMENTATION CENTER (DDC)
CAMERON STATION
ALEXANDRIA, VIRGINIA

Department of Defense contractors must be established for DDC services or have their 'need-to-know' certified by the cognizant military agency of their project or contract.

All other persons and organizations should apply to:

U. S. DEPARTMENT OF COMMERCE
OFFICE OF TECHNICAL SERVICES
WASHINGTON 25, D. C.

AFCRL-63-575

# PROMPT ACTIVATION ANALYSIS FOR BORON AND LITHIUM

Lincoln Clark, Jr.
Norman C. Rasmussen

Massachusetts Institute of Technology
77 Massachusetts Avenue
Cambridge, Massachusetts

Scientific Report No. 2

MITNE-42

Contract No. AF19(604)-7492

Project 4608
Task 460801

October 1963

Prepared for

Air Force Cambridge Research Laboratories
Office of Aerospace Research
United States Air Force
Bedford, Massachusetts

# ABSTRACT

## PROMPT ACTIVATION ANALYSIS FOR BORON AND LITHIUM

by

LINCOLN CLARK, JR.

Submitted to the Department of Nuclear Engineering on August 26, 1963, in partial fulfillment of the requirements for the degree of Master of Science.

Activation analysis for boron and lithium is not possible in the usual sense because neither one becomes radioactive under neutron irradiation. However, both have large thermal-neutron cross sections for the $(n,\alpha)$ reaction, and activation analysis is possible if one measures the prompt particles emitted.

Based on an analysis of the several types and sources of radiation which would be experienced, including background, it was decided to employ a gas-flow proportional counter. Optimum size for discrimination against electrons and betas is a sensitive volume one centimeter in diameter by one centimeter long. The walls of the chamber are made from the material to be analyzed and are thick enough to absorb heavy charged particles from the structural materials of the counter, thus reducing the background. The end of the counter is removable for changing samples. Neutrons for the $(n,\alpha)$ reactions were obtained for most of the work by exposure of the counter in the "hohlraum" of the MIT Reactor at a flux of $1.14 \times 10^8$ neutrons/$cm^2$-sec.

The device was calibrated by use of aluminum standards containing known amounts of boron or lithium. The difference in the energy spectra makes it possible to determine the relative amounts of these two elements and, in conjunction with the count rate, to find the concentration of each in aluminum. Approximate analyses of aluminum and graphite unknowns were made in the region of one part per million boron plus lithium. An analysis of background effects indicates that the method should be applicable at concentrations which are at least a factor of ten or one hundred lower.

Thesis Supervisor: Norman C. Rasmussen
Title: Associate Professor of Nuclear Engineering

## ACKNOWLEDGEMENTS

The writer wishes to express his appreciation to many personnel at the M. I. T. Reactor Project who were helpful in the work described in this report. Special thanks are due Professor N. C. Rasmussen, Thesis Supervisor, Professor T. J. Thompson, Reactor Project Director, Professor D. D. Lanning, Assistant Director, and the machine shop, electronics shop, and reactor operations personnel, all of whom generously contributed valuable assistance in the construction and operation of the equipment. Preparation of the report was primarily the work of Miss Constance Clark and Miss Mary E. Stuart.

# TABLE OF CONTENTS

# LIST OF FIGURES

# LIST OF TABLES

# SECTION I

# INTRODUCTION

## A. Activation Analysis of Light Elements

Activation analysis, as the name implies, is performed by activating the material of interest and then measuring the radiation which occurs as a result of the activation. Activation is accomplished by means of a nuclear transformation whereby a stable nuclide is converted through a known reaction into an unstable, or radioactive, nuclide. These, fortunately, emit radiation which is characteristic of the nuclide and which, on measurement, permits thereby an identification of the nature and amount of the original stable nuclide present in the sample being assayed.

The activation may be accomplished either with charged particles (usually protons, deuterons, or alphas) or with neutrons.

The availability of nuclear reactors, which furnish low-energy neutrons in great abundance, has stimulated interest in activation analyses by the $(n,\gamma)$ reaction, and hence a major part of the work in the field has been along the lines of neutron activation analysis. Also, there are today accurate and convenient devices for detecting and measuring the energy and quantity of the gamma radiation usually emitted when the end products of the $(n,\gamma)$ reaction eventually undergo decay. It is also possible to analyze the beta particles emitted in these decays, but such measurements are neither as convenient nor as precise as measurements of the gamma radiation. The Activation Analysis Group at Oak Ridge National Laboratory, in a six-year period ending in 1959, determined at least 70 of the elements in many different sample materials, mostly by the neutron activation method followed by gamma scintillation spectrometry. A tabulation of some of these applications, the concentrations observed, and the potential sensitivities, is given by Leddicotte, et al (1).

The well-investigated method of thermal neutron activation

plus gamma spectrometry is not amendable, however, to analysis of the light elements, as is indicated by the fact that Leddicotte's listing contains no report of work on elements lighter than oxygen. Also, Koch (2) gives no references to analyses using the $(n,\gamma)$ reaction for the light elements up to and including oxygen. The reasons are apparent from a study of the nuclear properties (3) of the light elements, summaries of which are provided for convenience in Appendices A and B. Only a few neutron capture processes, essential to the formation of radioactive nuclides which decay by $\beta^-$ and gamma emission, are seen to occur. Furthermore, for the $(n,\gamma)$ reactions, listed in Appendix A, the product in most cases is either stable or decays by $\beta^-$ emission with no gamma. Where gamma's are emitted, the half-life is very short (0.022 seconds for $B^{11}(n,\gamma)B^{12}$) or the yield is very low (as in the cases of $N^{15}(n,\gamma)N^{16}$ and $O^{18}(n,\gamma)O^{19}$) due to low natural abundance of the nuclides involved and their small thermal neutron cross sections.

For other neutron capture reactions, (n,p) and n,$\alpha$), as shown in Appendix B, no gamma-emitting nuclides are formed, and hence gamma spectrometry is again impossible.

The reactions listed in Appendix B may, however, be used directly. Various means are available for recording the products of the (n,p) and $(n,\alpha)$ reactions. The material of interest may be exposed to thermal neutrons while in contact with photographic film. Mayr (4) (5) used this method to determine the boron in tissue, exposing the sample, while in contact with NTA emulsion, to a Po - Be neutron source and then counting the alpha tracks.

Another means of detecting these light elements is to count the reaction products directly with an electronic counting device. Wanke and Monse (6) employed a 100 mc Ra - Be neutron source in a paraffin moderator to produce thermal neutrons for the reactions $Li^6(n,\alpha)H^3$, $B^{10}(n,\alpha)Li^7$, and $U^{235}$ (n,f). An "infinitely thick" layer (thicker than the range of either reaction product in the film material) containing a compound of the element to be measured was placed in contact

with a ZnS screen serving as the phosphor on a photomultiplier tube. Pulses from the heavy, ionizing particles were counted, while the small gamma pulses from the radium source were eliminated by means of a discriminator. The objective here was to determine the isotopic abundance of $Li^6$, $B^{10}$, and $U^{235}$.

Fiti, Mantescu, and Costea (7) used a somewhat similar arrangement to measure boron in minerals. They reported the determination of concentrations from 15 per cent, with a 0.26 per cent error, to 0.05 per cent, with a 10 per cent error. They pointed out that the sensitivity of the method could be increased by use of high neutron flux with proper protection for the phototube.

Kienberger, Greene, and Voss (8) have used a similar method to determine $Li^6/Li^7$ ratios. Detection of the prompt alpha and $H^3$ particles was again accomplished with a scintillation counter.

B. Objective of This Investigation

In the last three investigations referred to above, thermal neutron fluxes on the order of $10^2$ - $10^3$ $n/cm^2$-sec. were obtained by moderating with paraffin or graphite the fast neutrons from Po - Be or Ra - Be sources. As suggested by Fiti, et al, (7) it should be possible to increase the sensitivity of the method by use of high neutron fluxes.

The objective of the experimental work for this report has been to design and operate a detector capable of utilizing the high fluxes ($10^9$ - $10^{10}$ $n/cm^2$-sec.) in the thermal column and in the medical therapy room beam of the Massachusetts Institute of Technology Research Reactor (MITR). The purpose of this particular detector is to measure trace quantities of two of the light elements, lithium and boron, by direct counting of the prompt particles from the reactions, $Li^6(n,\alpha)H^3$ and $B^{10}(n,\alpha)Li^7$. It was also hoped that it would be possible, by analysis of the energy spectrum of the particles, to distinguish between the two reactions.

Since one of the limitations of measurements for trace impurities arises from interference by small amounts of similar

elements occurring as impurities in the structural material of any counter that may be fabricated, it was decided at the outset to design a counter which would have a chamber lined sufficiently thick with the material to be assayed for B and Li that alpha and $H^3$ particles from other B and Li impurities would not be able to penetrate into the chamber. This, and other design considerations, led to the selection of a gas-flow, proportional counter as the type of detector to be constructed.

For the experimental work, only one chamber-lining material--aluminum--containing known amounts of boron and lithium was used in evaluating the feasibility of the method and in calibrating the counter constructed. A few runs were also made with a graphite matrix.

## C. Sensitivities of Charged-Particle Activation and Spectrochemical Analysis

For purposes of comparing the sensitivities attainable by neutron activation analysis with those reported for other methods, mention of two investigations should be made here.

Gill (9) describes the use of the Harwell Cyclotron to determine trace amounts of boron in silicon, an analytical problem of interest in the semiconductor field. By counting the 0.51 Mev gammas from the $\beta^+$ decay of $C^{11}$ and $P^{30}$, produced by $B^{11}(p,n)C^{11}$ and $Si^{30}(p,n)P^{30}$, it is possible to determine the ratio $C^{11}/P^{30}$ with sufficient accuracy so that 0.003 ppm boron in silicon can be detected.

Davis, et al, (10), describes the use of a high sensitivity flame photometer. Sensitivities for various elements are given, including a minimum detectable weight for lithium of $8 \times 10^{-11}$ grams and a minimum detectable concentration of 0.5 ppb.

Also, in a description of the historical development of spectral analysis, Lipis (11) uses boron to illustrate the increase in sensitivity of this method from $10^{-2}$ per cent in 1946 to $10^{-8}$ per cent in 1957.

# SECTION II

# DISCUSSION OF PROBLEM

## A. General Considerations

The design of the detector for measuring boron and lithium was based on consideration (1) of the desirability of operating the detector in the reactor at moderately high neutron fluxes with a capability for frequent changing of samples and (2) of the various types of ionizing radiations which would be encountered.

The first consideration required the use of materials for structural and electrical purposes which would withstand thermal neutron fluxes on the order of $10^{10}$ neutrons/$cm^2$-sec. and gamma fluxes on the order of a few hundred roentgens/hour. For comparatively short exposures to these dose rates, radiation damage is not an important factor. It would be if the detector were to be operated in the core of the reactor at fluxes in excess of $10^{13}$ neutrons/$cm^2$-sec. and $10^8$ r/hour for gammas (12). Although the possibility of radiation damage, therefore, imposed few limitations, the need to change samples frequently did affect the choice of materials and the design. The use of complicated shielding devices was avoided by making the counter small and constructing it primarily from materials which do not activate appreciably (e.g. polyethylene) or which have short half-lives (e.g. aluminum). (The use of a small detector was dictated basically by other considerations, as explained below.) This permitted removing the detector from the reactor after a brief cooling period, in order to change the sample. Materials that activate like Cu were avoided entirely or kept to a minimum.

The need to operate the detector in moderately high fluxes and to remove it for sample changing presented problems in connection with the use of certain types of devices such as the scintillation detector, so that they appeared to have no particular advantages in comparison with a gas-flow

proportional counter.

A review of the types of radiation which are encountered in a detector operated under these conditions provides further information on the relative suitability of other counters for this task.

## B. Types of Ionizing Radiation in Detector

When B and Li react with thermal neutrons, they promptly emit heavy ionizing particles, and it is these which are to be detected and used as a measure of the amounts of B and Li present in the material. In addition, however, there are a number of other interfering sources of ionizing radiations which must be taken into account. Both types are listed in Table II-1; items 1-4 are the particles of interest, while items 5-11 are the interfering radiations. (See following page.)

## C. Detector Design

The design objective now consisted of maximizing the counter response to one or both of Items 1 and 2 and to one or both of Items 3 and 4. At the same time the response to Items 5-11 should be minimized.

The necessity of preserving the ionization-pulse height relationship and the desirability of using gas amplification led to the choice of a proportional counter. Because alpha-particle energies were to be measured and for a second reason discussed below, samples had to be placed inside the detector, and the need to change these samples frequently dictated the use of a gas-flow proportional counter.

Use of a proportional counter provides the opportunity to discriminate against the small background pulses caused by secondary electrons and beta rays, in favor of the larger pulses from alphas and other heavy particles. In high fluxes of betas and gammas, however, a limitation is reached when the background of betas and gammas becomes so high that pulse pile-up interferes with the alpha counting. In this application, therefore, it is important to obtain the maximum possible ratio of heavy-particle pulse size to electron or beta pulse size.

## TABLE II-I

## IONIZING RADIATIONS EXPECTED IN COUNTER

| Item | Particle | Source |
|---|---|---|
| 1. | $\alpha$ | B to be measured, by reaction $B^{10}(n,\alpha)Li^{7}$ |
| 2. | $Li^{7}$ | B to be measured, by reaction $B^{10}(n,\alpha)Li^{7}$ |
| 3. | $\alpha$ | Li to be measured, by reaction $Li^{6}(n,\alpha)H^{3}$ |
| 4. | $H^{3}$ | Li to be measured, by reaction $Li^{6}(n,\alpha)H^{3}$ |
| 5. | Electrons | Primarily Compton and photoelectrons from gamma rays of capture, decay, and the reactor core. |
| 6. | Beta rays | Decay of radioactive nuclides (such as $Al^{28}$) formed in matrix of sample or in structural materials of detector. |
| 7. | $\alpha$, $Li^{7}$, $H^{3}$ | B and Li present as impurities in structural materials of detector. |
| 8. | $\alpha$ | Uranium and other naturally radioactive nuclides present as impurities in sample and in structural materials of detector. |
| 9. | Fission fragments | Uranium present as an impurity in the sample and in structural materials. |
| 10. | Recoil nuclei | Collisions between fast neutrons and light nuclei of sample and structural materials. |
| 11. | $\alpha$, $Li^{7}$, $H^{3}$ | Contamination of sample or other interior surfaces with impurities containing boron or lithium. |

The heavy-particle ionization will be a maximum when all of the energy of the particle is expended within the sensitive volume of the detector. Fortunately, the ranges of such particles do not exceed a few centimeters in gases at atmospheric pressure, so detectors of such dimensions are reasonable. It is desirable that the end of a particle's flight be within the counter, since the Bragg specific ionization curve shows that the number of ion pairs formed per unit length is greatest near the end of the range. Secondary electrons and beta rays, on the other hand, even those with moderate energies, may travel several meters, so that each one will give up only a fraction of its energy within a gas-filled detector. The optimum condition then occurs when the sensitive volume of the detector is just large enough to contain the maximum range of the heavy particles but no larger, so that electrons and betas will give up a minimum of their energies.

A study of the energies and ranges of the products of the reactions of interest, $B^{10}(n,\alpha)Li^7$ and $Li^6(n,\alpha)H^3$, yields an indication of what the chamber size should be. The $B^{10}(n,\alpha)Li^7$ reaction has a disintegration energy of 2790.1 ($\pm$1.1) Kev (13), or 2.79 Mev, where the product nuclei are left in the ground state in only 6.52 per cent of the cases (14). 93.48 per cent of the time, the disintegration energy is 2.31 Mev. The $Li^7$ nucleus is produced in an excited state, but it immediately goes to the ground state with emission of a 0.477 Mev gamma ray. For the $Li^6(n,\alpha)H^3$ reaction, the disintegration energy is 4786.4($\pm$1.1) Kev (13), or 4.79 Mev. Data on these reactions is tabulated below. Values for the last two columns are based on the experimentally known ranges of alpha particles in air, adjusted by the usual relationships to account for different properties of the ionizing particle and the material traversed.

From the table below, and on the assumption that a counting gas is used for which the particle ranges are similar to those in air, it appears that a chamber with dimensions on the order of one centimeter will permit all particles except the tritons to expend their entire energies within the confines

of the chamber. As it turns out, it is advantageous to size the detector so that the tritium does not give up all of its energy within the chamber.

TABLE II-2

ENERGIES AND RANGES OF REACTION PRODUCTS

| Isotope and Natural Abundance | Reaction and Cross Section | Product Particles | Kinetic Energy (Mev) | Range in Air (cm.) | Range in Al (cm.) |
|---|---|---|---|---|---|
| $B^{10}$ 18.7% | $B^{10}(n,\alpha)Li^7$ 4000 b. | $\alpha$ | 7% 1.78 | 0.89 | $0.55(10^{-3})$ |
| | | | 93% 1.47 | 0.73 | $0.45(10^{-3})$ |
| | | $Li^7$ | 7% 1.01 | 0.26 | $0.16(10^{-3})$ |
| | | | 93% 0.84 | 0.24 | $0.15(10^{-3})$ |
| $Li^6$ 7.5% | $Li^6(n,\alpha)H^3$ 945 b. | $\alpha$ | 100% 2.06 | 1.03 | $0.64(10^{-3})$ |
| | | $H^3$ | 100% 2.73 | 6.02 | $3.7(10^{-3})$ |

D. Anticipated Counting Rates From All Sources

In order to obtain an indication of how the interfering radiations listed in Table II-1 might limit the sensitivity of the detection system, estimates were made of the counting rates which might result from each source of radiation. For these estimates it was assumed that the chamber was lined with aluminum at least $3.7 \times 10^{-3}$ cm. thick. This material was selected for the calculations because it was the one most extensively used for the experimental work, and this thickness was chosen because it is equal to the range in aluminum of the 2.73 Mev tritons from $L^6(n,\alpha)H^3$, the longest range of the heavy particles to be counted.

For purposes of calculation, one part per million (1 ppm) by weight of boron or of lithium was assumed to be present, and a thermal neutron flux of $10^8$ $n/cm^2$-sec. was used. The following Table II-3 summarizes the data.

## TABLE II-3

## SUMMARY OF ANTICIPATED EFFECTS OF IONIZING RADIATIONS

| Item | Particle | Source | Kinetic Energy (Mev) | Ranges (cm.) | | Estimated $CPM/ppm\text{-}cm^2$ at flux of $10^8 n/cm^2\text{-}sec$ |
|---|---|---|---|---|---|---|
| | | | | Air | Al | |
| 1. | $\alpha$ | $B^{10}(n,\alpha)Li^7$ | 1.47(93%) | 0.73 | $0.45 \times 10^{-3}$ | 101 |
| 2. | $Li^7$ | " | 0.84(93%) | 0.24 | $0.15 \times 10^{-3}$ | |
| 3. | $\alpha$ | $Li^6(n,\alpha)H^3$ | 2.06 | 1.03 | $0.64 \times 10^{-3}$ | 108 |
| 4. | $H^3$ | " | 2.73 | 6.02 | $3.7 \times 10^{-3}$ | |
| 5. | $e^-$ | $\gamma$'s | .002-.032/cm. of air | $0\text{-}10^3$ | 0-1 | ~ 0(Discrim.) |
| 6. | $\beta$ | Al decay | .002-.032/cm. of air | $0\text{-}10^3$ | 0-1 | ~ 0(Discrim.) |
| 7. | $\alpha$ | B + Li in | as above | as above | as above | Low |
| | $Li^7$ | structural | " | " | " | Low |
| | $H^3$ | materials | " | " | " | Low |
| 8. | $\alpha$ | $U^{238}$, etc. | 5 | 3.5 | $2.2 \times 10^{-3}$ | 0.003 |
| 9. | f.f. | $U^{235}(n,f)$ | 81 av. | 2.3 av. | $1.4 \times 10^{-3}$ av. | 0.013 |
| 10. | recoil nuclei | fast neutrons | depends on energy spectrum of fast flux | | | |
| 11. | $\alpha$, $Li^7$, $H^3$ | surface contamination | as above | as above | as above | no estimate |

The kinetic energies of the various particles are listed in the fourth column, except for the electrons and beta rays, where the calculated range of energy loss per centimeter of air is given. The estimates of counting rates, where figures are given in the righthand column, were later shown by the experimental runs to be of the proper order of magnitude. Where no quantitative estimates are given, indications of the magnitude of the interference were obtained in the experimental work, and these are discussed below under Section IV-E.

The problem of reducing background due to Item 7, the $\alpha$, $Li^7$, and $H^3$ particles entering the chamber as a result of $(n,\alpha)$ reactions by boron and lithium present as impurities in the structural materials of the detector, was partially overcome by lining the chamber with the material to be assayed. This could most easily be accomplished by using a cylindrical detector and lining the cavity with a sleeve fabricated from the material being tested. By using a central electrode supported only at one end, it was possible to close the other end of the sleeve, again with the material being tested. Heavy particles from impurity boron and lithium in the structural materials (other than the test sample) could then enter only from the anode or from the material holding the anode in position.

For the counting gas, a mixture of 90% argon-10% carbon dioxide was used because its constituents have low electron attachment coefficients, reasonably high drift velocities, sufficiently high atomic weights so that recoil nuclei were not a problem (as they would be for 90% argon-10% methane, for instance), a comparatively low operating voltage, reasonably low neutron activation, and chemical inertness (15). The ranges of the $\alpha$, $Li^7$, and $H^3$ particles to be counted are 16% greater in the A-$CO_2$ mixture than they are in air (Table II-2).

## SECTION III

## FABRICATION

The counter which resulted from the above design considerations and which was used for most of the experimental work in this investigation is shown in Fig. 1. It is cylindrical in shape, has a diameter of 0.610", because it was necessary that it fit into a 0.620" bent tube in the thermal column of the MITR. This proved just large enough to accommodate a cavity with a diameter of 1 cm. The anode is a 0.002" tungsten wire, 1 cm long, so that the sensitive length of the detector is approximately 1 cm.

In order to permit sample changing, the anode is supported at only one end. The aluminum plug at the right hand end of the drawing unscrews so that a sample of the size shown in Fig. 1b may be inserted into the cavity. In this manner, the sample material itself forms the inside surface of the counting chamber and almost completely surrounds the anode. It was found that the anode wire was stiff enough for this application, but it had the disadvantage that the wire was not stretched tight and was not supported precisely on the center axis. A spherical covering was provided to cover the sharp end of the anode wire which otherwise would be a region of very high gas multiplication. It was found that sulfur had the property of adhering to the wire and of assuming a spherical shape when melted. It was covered with aquadag to make it conducting.

The shell of the counter was machined from Type 1100 aluminum. In order to avoid galling of the outer surface, it was covered with a hard coating of aluminum oxide, 0.002" thick, by an electrolytic process known as "Duralectra."

A combination aluminum and polyethylene plug screws into the left hand end of the shell. A 7 ft. length of Aljak No. 21-607 coaxial cable is fixed in position in the aluminum portion of this plug. This cable has an aluminum jacket which, while providing some flexibility, reduces the activation which would otherwise result in standard coax when it is exposed to

6/11/63

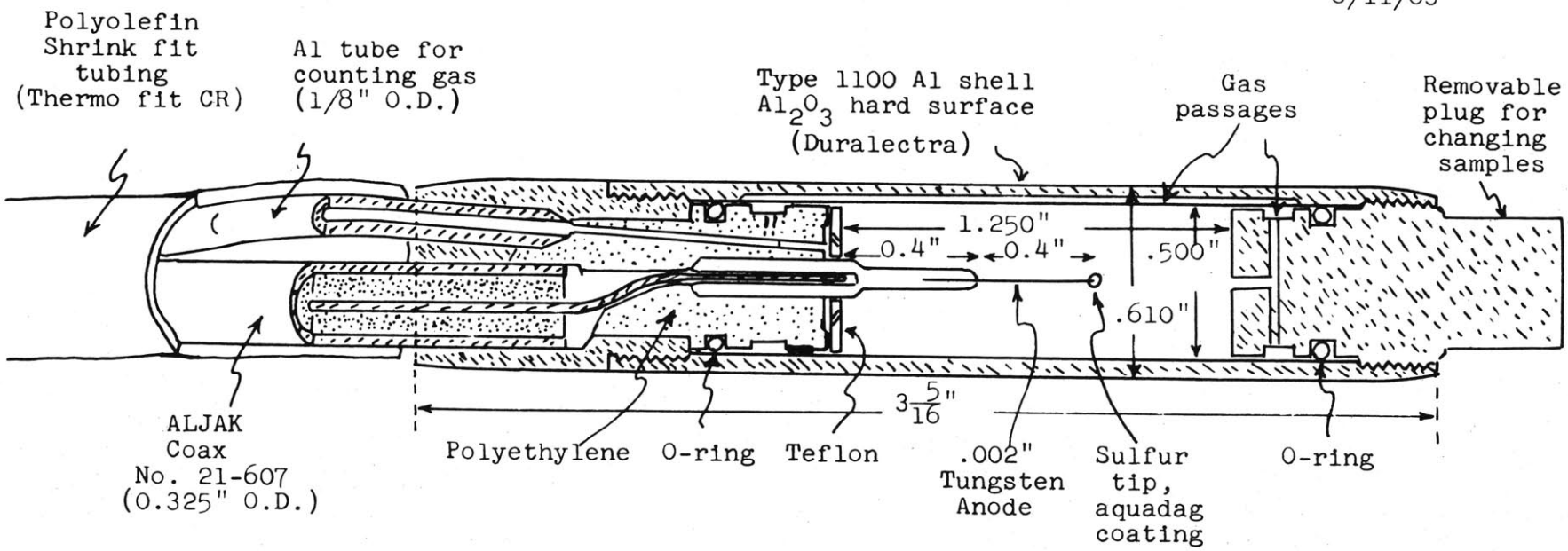


FIG. 1a. DRAWING OF GAS-FLOW PROPORTIONAL COUNTER

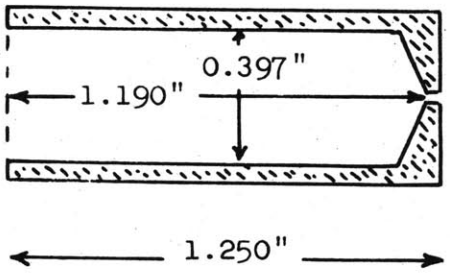


FIG. 1b. STANDARD SAMPLE

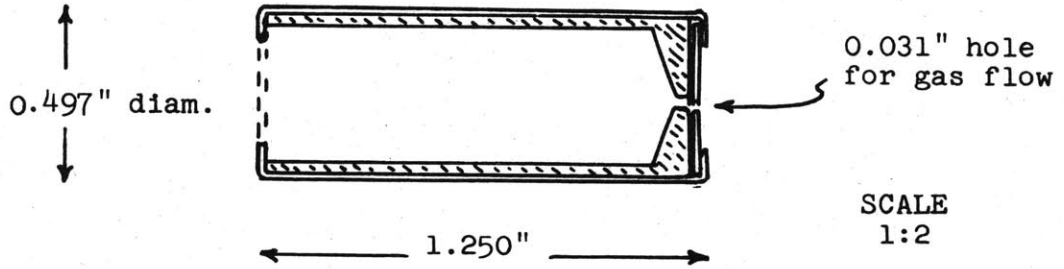


FIG. 1c. CADMIUM-WRAPPED SAMPLE

neutrons. The center conductor is copper, but it did not build up to troublesome activities during the test runs. The center conductor passes through the polyethylene portion of the plug to an aluminum rod which serves to join it electrically to the anode and also to support the latter in position. This support extends about 1 cm into the cavity, so that heavy ionizing particles from boron or lithium impurities at the end of the chamber will not reach the sensitive portion. A teflon wafer separates the polyethylene from the chamber, so that recoil protons cannot enter.

The counting gas is brought to the chamber through one of a pair of 1/8" O.D. aluminum tubes. The gas passes through a drill hole in the polyethylene to a circular groove in the face of the plug. 0.031" diameter holes are provided in the teflon wafer and are drilled at an angle so that any knock-on protons passing through them will be directed toward the anode support. Electrons from any ionization which occurs inside the chamber should be collected without multiplication on the anode support. The gas then passes through the chamber, out through a .031" hole at the end, through passages in the end plug, and back around the outside of the chamber by means of several grooves cut on the inside surface of the counter shell. It leaves the counter through a circumferential groove in the polyethylene, two drill holes, and the other piece of aluminum tubing. Buna N O-rings provide gas seals at both ends of the counter shell. The gas was under a pressure of a few inches of water. Epoxy resin was used to improve the gas tightness of the joint where the coax and the aluminum tubing enter the counter. Expanded polyolefin tubing (Thermofit CR) was heat shrunk over the coax and aluminum tubing, which provided a smooth, non-galling surface and which made it easier to slide the counter through the bent tube which passes through the reactor shielding.

Most of the samples used in the test runs were made from aluminum spectrochemical standards, purchased from the Aluminum Company of America. One set of standards contained known amounts of boron, ranging from 5 to 290 parts per million. A second set contained lithium ranging from 5 to 280 parts per million.

It was arbitrarily assumed that there was a standard error of 5 parts per million in the analyses furnished by the company.

Two cylinders of the type shown in Figure 1b were machined from each of the standards. Since the surfaces undoubtedly became contaminated during the machining operations, the finished pieces were etched for about 5 minutes at 70-75° C in a 3.7% hydrochloric acid solution. They were rinsed with distilled water, soaked in acetone, given a final rinse in acetone, drained and dried.

In addition to the aluminum standards described above, cylinders were also made from an aluminum blank obtained from ALCOA and from a 99.9999% aluminum ingot, the boron and lithium contents in both cases being unknown.

In hopes of finding a material which would have lower boron or lithium content than the aluminum, graphite from two sources was used for making additional samples. Two pieces were machined from a bar of reactor grade graphite. In addition, two bars of graphite manufactured by National Carbon Company for use as spectroscopic electrodes were used to make additional samples.

In order to determine, if possible, the extent of the background caused by recoil nuclei, the thermal flux entering the cavity was reduced as much as possible by wrapping several of the standards in 0.020" thick cadmium. A cylinder of this type is illustrated in Figure 1c.

The characteristics of the detector were determined with an alpha source which had been made by depositing about $10^{-4}$ grams of $U^{235}$ in the form of $U_3O_8$ on an aluminum foil, which was then fitted to the inside of a cylinder drilled to the same dimensions as the standard samples described earlier.

In order to determine whether or not the counter might be overloaded by a high flux of secondary electrons, a gold-lined sample was also fabricated. Since gold has a high atomic number, the density of photoelectrons is greatly enhanced over that for an all-aluminum chamber. The gold was 0.006" thick, and so an aluminum cavity was made in the usual manner except that the inside diameter was 0.012" larger than normal in order to allow for the thickness of the gold. Photographs of the counter and samples appear in Figure 2.

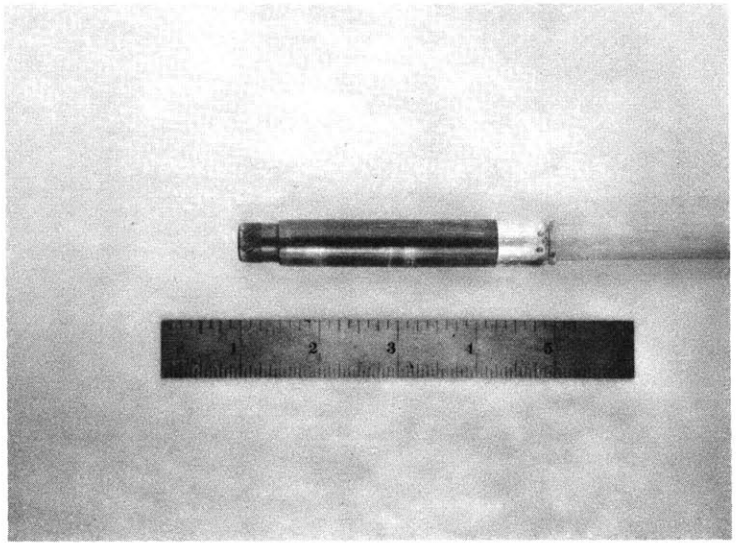

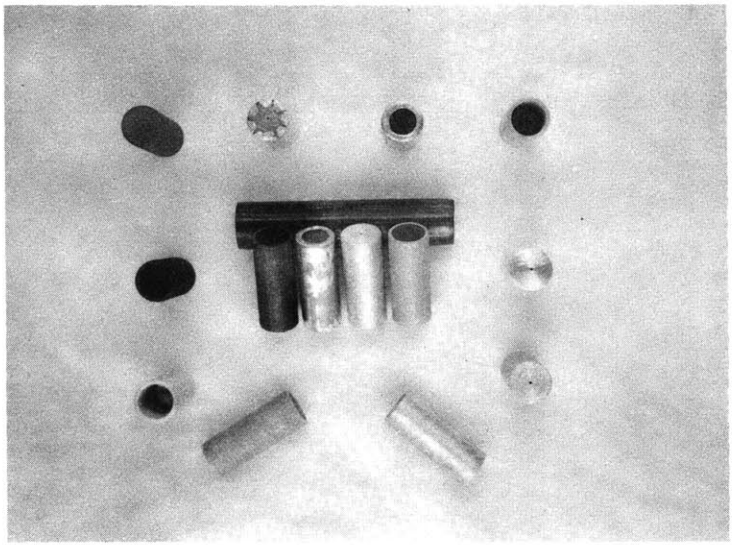

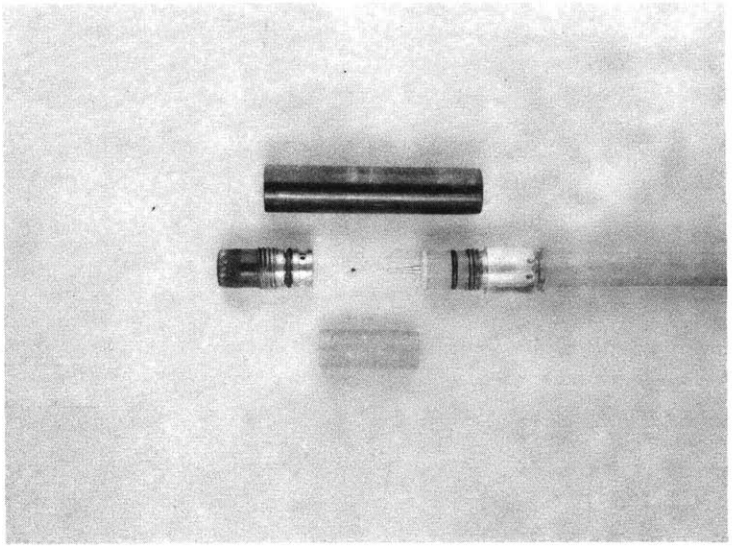

FIG. 2 GAS-FLOW PROPORTIONAL COUNTER

a.(Upper Left) ASSEMBLED COUNTER.

b.(Lower Left) DISASSEMBLED; REMOVABLE END PLUG AT LEFT, SAMPLE TO BE COUNTED AT BOTTOM.

c.(Upper Right) ALUMINUM AND GRAPHITE SAMPLES READY FOR OPERATION IN COUNTER (SOME SAMPLES CADMIUM WRAPPED).

# SECTION IV

# OPERATION

## A. Instrumentation

The following electronic equipment was employed:

Proportional amplifier - Baird-Atomic, Inc., Model 255

Scaler - Baird-Atomic, Inc., Model 132

Oscilloscope - Tektronix, Inc., Model 541

Pulse height analyzer - Technical Measurement Corporation, Model CN-110

The linearity of the above system was determined by introducing a calibrated, negative pulse to the preamplifier input, measuring the output to the analyzer with the oscilloscope, and noting the channel in which the pulses (most of them) were stored. A Radiation Counter Laboratories Precision Pulse Generator, Model 20900, was used to supply the calibrated pulse (60 cps, about 1 μs rise time, 20 ms decay, and 0 - 100 mv amplitude). On recording the preamplifier output (TMC input) and TMC channel number as shown in Figure 3, the curves indicate good linearity up to 12 - 14 mv, beyond which saturation in the preamplifier (or possibly an impedance change in the input circuit of the scaler, the scope, or the analyzer) causes the curves to flatten out. This was considered to be of no consequence, since data was collected primarily in the analyzer channels up to No. 60 or 70.

## B. Irradiation Facilities

Most of the experimental data was obtained during exposure of the counter to neutron fluxes in the "hohlraum" of the MIT Reactor. Preliminary runs were made in the neutron beam of the medical therapy room below the reactor. The standard pile of the Nuclear Reactor Physics Laboratory was also used for preliminary work and later for calibration of the detector and thus of the neutron fluxes in the pile oscillator tube.

The "hohlraum" is a flux-shaping, graphite-lined cavity (16) at the end of the reactor thermal column. A section through the reactor and the exponential facility is shown in Figure 4.

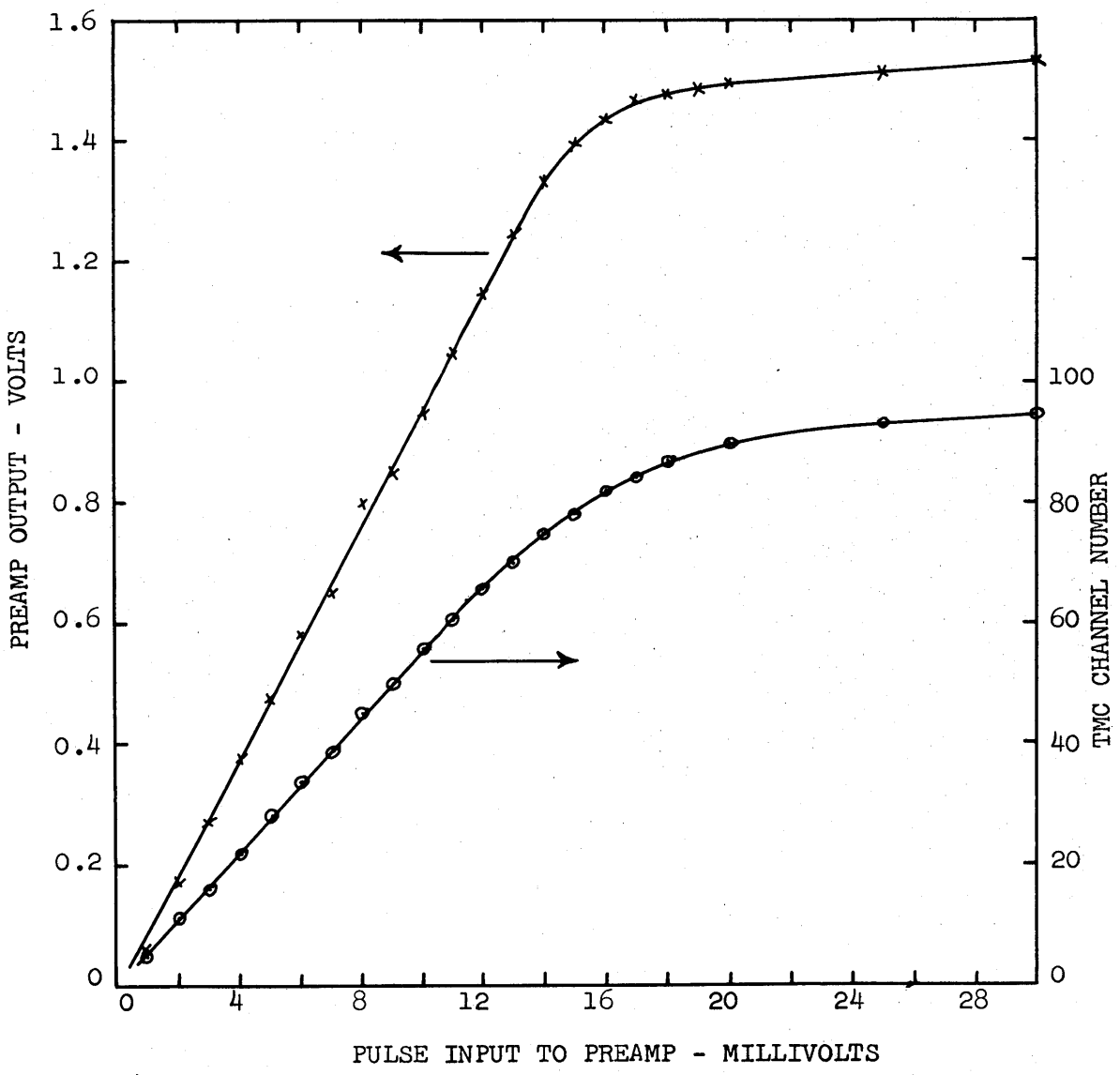


FIG. 3 SYSTEM LINEARITY (MOD. 255 PROPORTIONAL AMPLIFIER, MOD. 132 SCALER, TEKTRONIX SCOPE, AND TMC ANALYZER) (July 12, 1963)

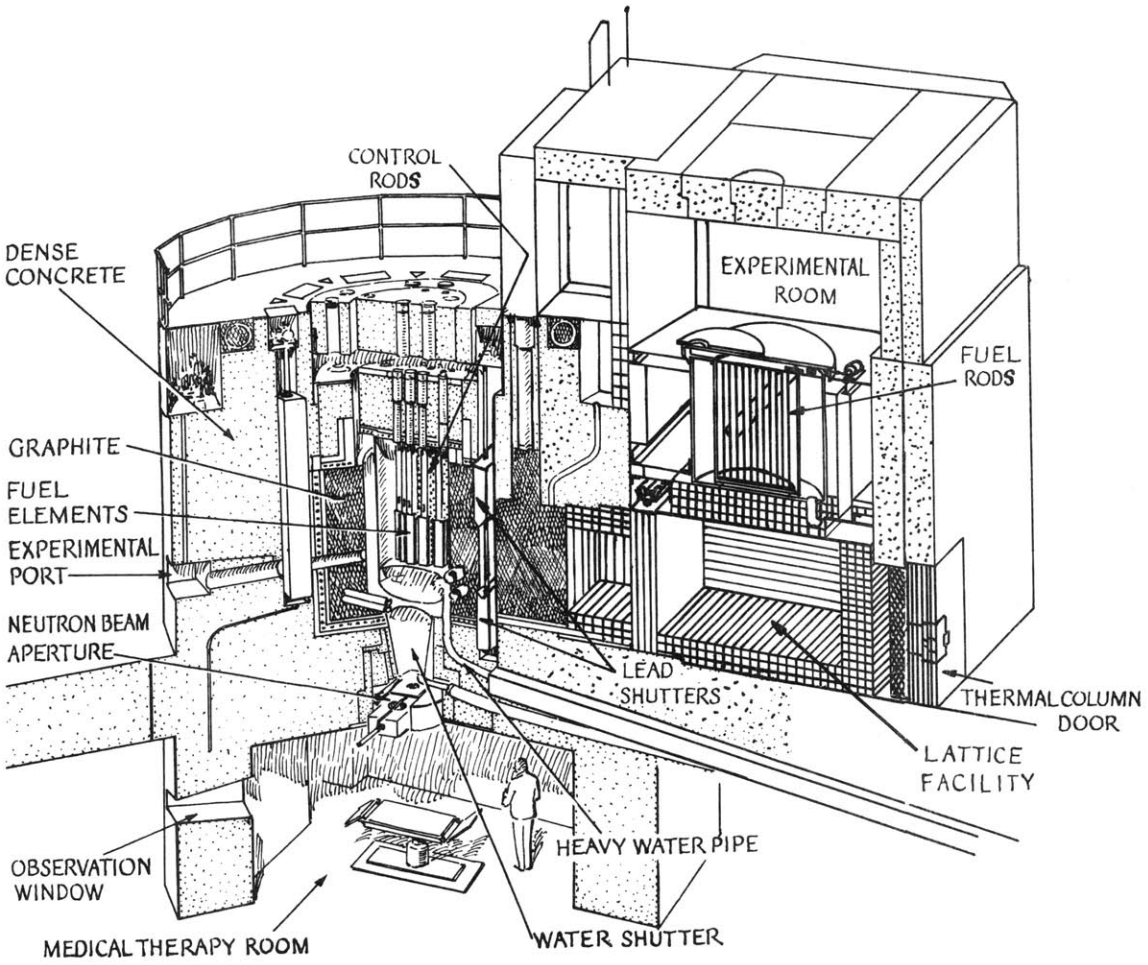


Fig. 4 **View of M.I.T. Research Reactor Showing Major Components and Experimental Facilities**

The original thermal column has been extended by adding a heavy water exponential facility of that side of the reactor. Neutrons from the core diffuse through 14" of graphite, across a 10" gap, through 38" of graphite, and finally into an empty space which has roughly the shape of a parallelepiped. The empty volume is 130" long, 72" wide, and, for the most part, 60" high. For the last 72", the two sides and bottom are lined with graphite 12" thick, and the end has a lining 16" thick. The purpose of the hohlraum is to cause neutrons coming from the thermal column to diffuse upwards through another graphite layer, 16" thick, at the top of the cavity, into a heavy water exponential tank situated above the hohlraum. Figure 5 is a horizontal section through the reactor core and the exponential facility. It also shows the lattice tank, which is actually located several feet above the level of the reactor core and the hohlraum.

The pile oscillator tube is located in a shielding plug in a port labelled 12CH1 in Figure 5. An aluminum tube, illustrated in Figure 6 and Figure 7, extends 32" through the biological shield, 18" through an air space between the shielding and the graphite lining of the hohlraum, 16" through the graphite, and then for 4 1/8" into the cavity. The total tube length, from shield face to the end in the hohlraum, is 70 1/8". The interior length is 69 3/8", due to a plug at the hohlraum end, and it has an inside diameter of 0.620". The outer end of the tube, where it passes through the shielding, is bent somewhat to prevent radiation streaming. This permits the insertion and removal of samples, including the detector, without a need for plugs or other shielding devices. Calibration of the thermal flux in the oscillator tube will be described below in this subsection.

The neutron beam of the medical therapy room was used for the initial exposures of an early model of the counter to relatively high flux levels, $10^9$ - $10^{10}$ neutrons/cm$^2$-sec. This was a convenient facility for the preliminary work, since this model was too large to fit into the oscillator tube. Integral bias curves were run for the aluminum standards containing 25 and 290 ppm boron, and for the reactor-grade graphite.

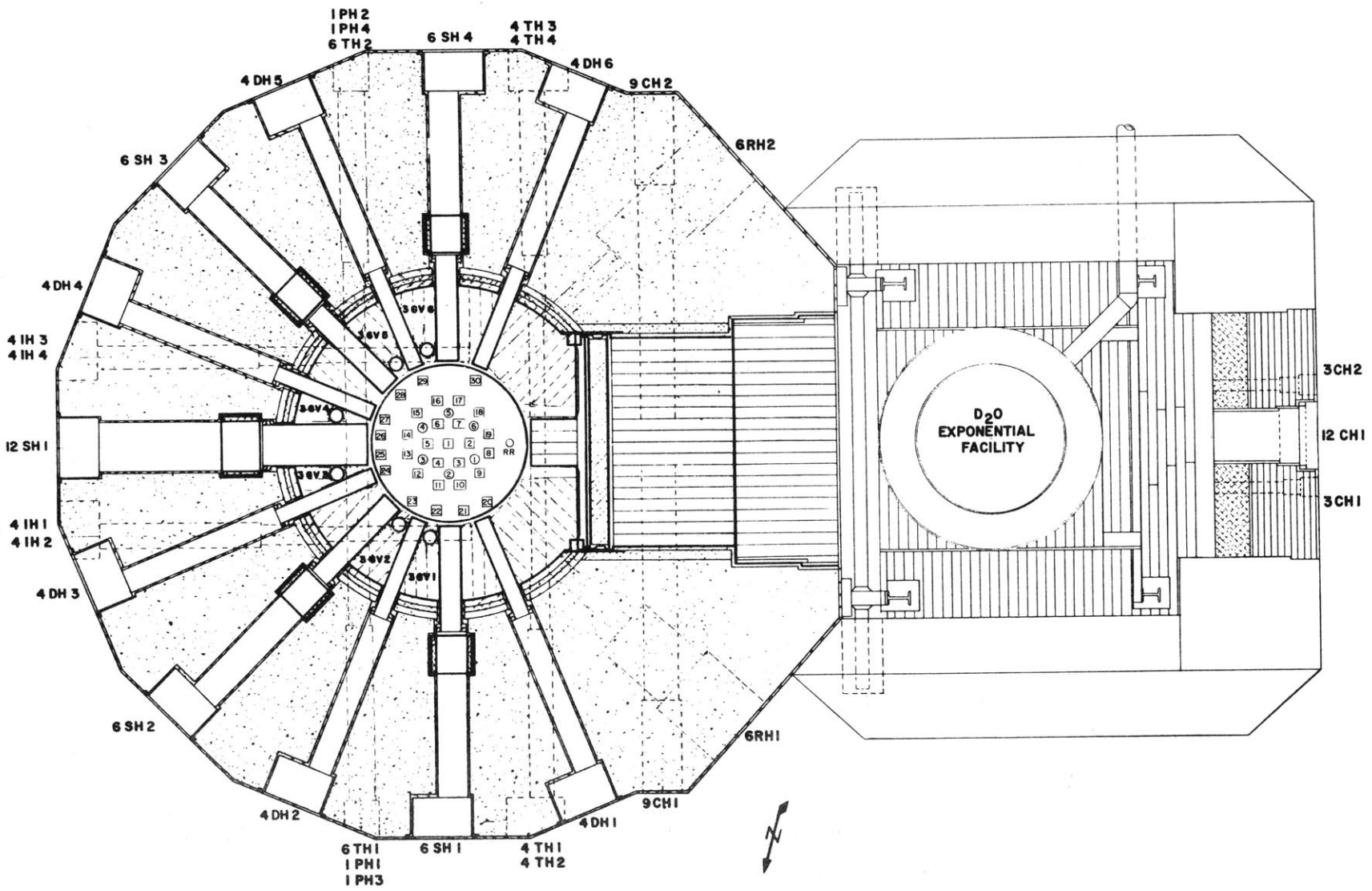


FIG. 5 HORIZONTAL CROSS SECTIONS THROUGH THE REACTOR AND EXPONENTIAL FACILITY.

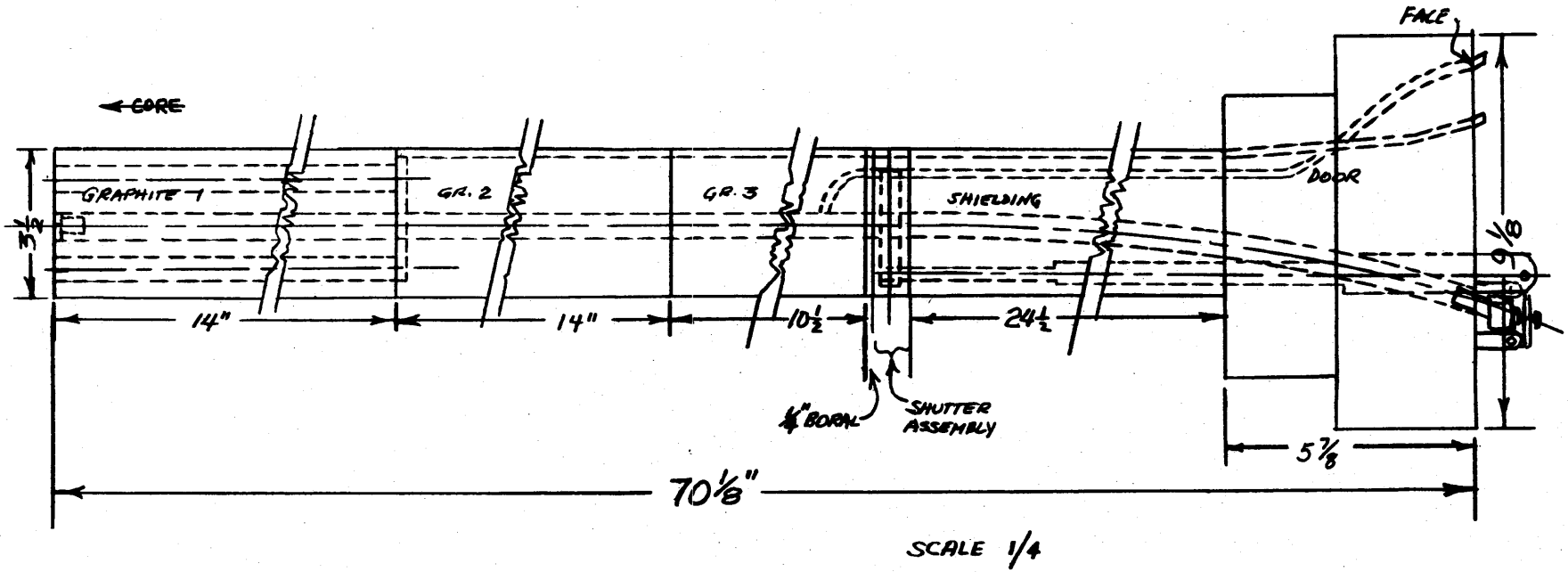


OVERALL ASSEMBLY

FIG. 6 PILE OSCILLATOR TUBE, GRAPHITE STRINGER, AND SHIELDING (FROM REFERENCE 22)

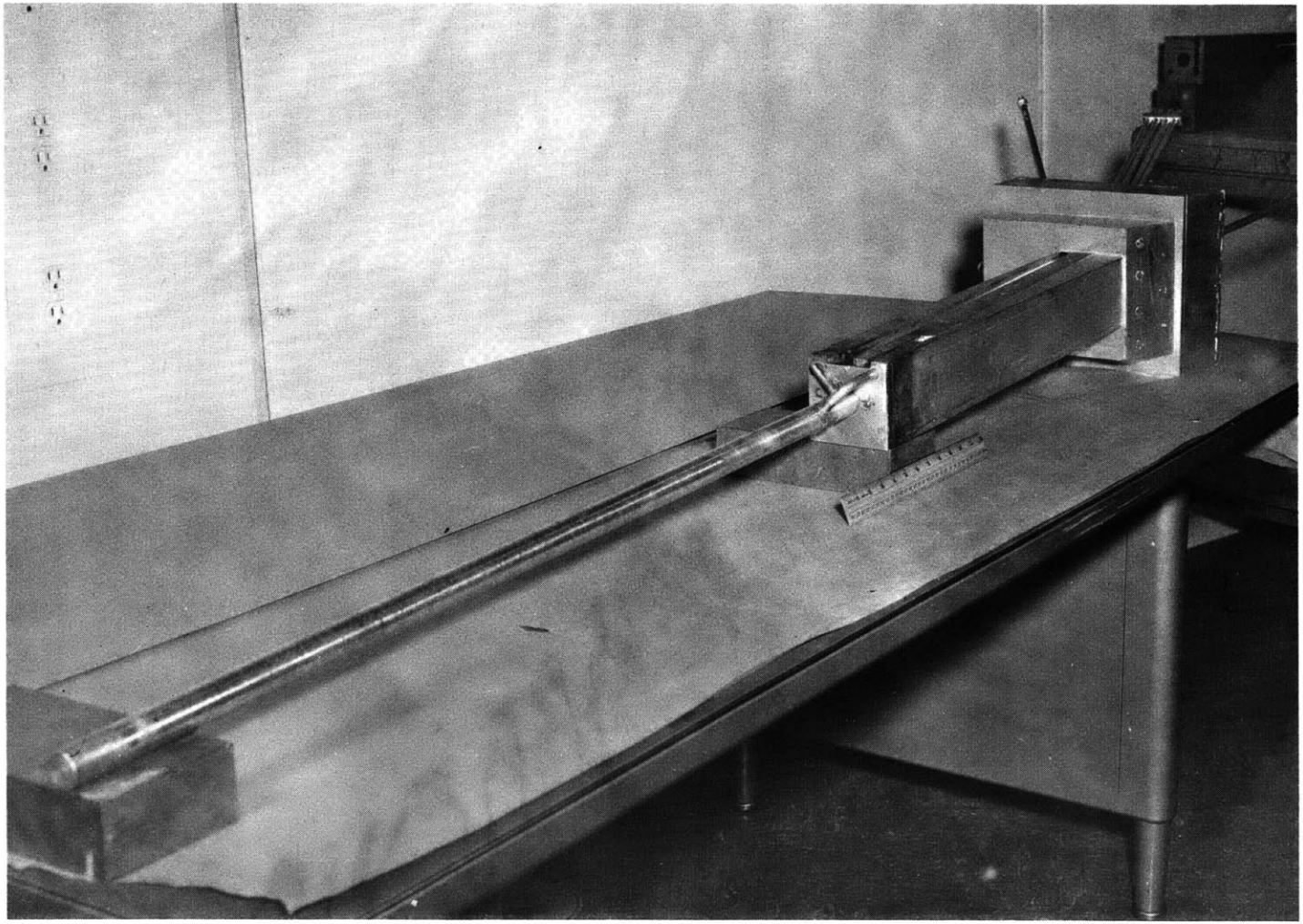

FIG. 7 PHOTOGRAPH OF PILE OSCILLATOR TUBE, GRAPHITE STRINGER REMOVED. (FROM REFERENCE 22)

The standard pile in the Nuclear Reactor Physics Laboratory (18) was very useful for the initial work in checking out the operation of the counters and later in providing a calibration for the counter, which was then used to calibrate the thermal neutron flux in the pile oscillator tube.

The standard pile is illustrated in Figure 8. It is constructed of nuclear-grade graphite stringers, recessed at appropriate points to permit insertion of foils, counters, and neutron sources. It is 86.5" high and has a 60" x 60" horizontal cross section. It is covered with a 0.020" cadmium sheath to reduce room return.

Neutrons for the standard pile were obtained from several (up to a maximum of five) plutonium-beryllium neutron sources inserted 13" up from the base of the assembly. Each source had one curie of plutonium and emitted approximately $1.6 \times 10^6$ neutrons per second.

For purposes of calibrating the counter, it was equipped with the aluminum standard containing 290 ppm boron and then exposed in each of two locations in the standard pile. The flux levels in these positions had previously been measured by Reilly (18) and found to be as follows:

| Position No. | Distance Above Source | Thermal Neutron Flux |
|---|---|---|
| 5 | 34.0 | $6.30 \times 10^{-3}$ |
| 11 | 89.3 | $1.04 \times 10^{-3}$ |

The counter was calibrated in both of these positions in order to determine whether or not fast neutrons from the sources might have a significant effect. If there was such an effect, it was obscured by variations in other conditions. The energy spectra of particles counted by the detector during the calibration runs in the standard pile are given in Figure 9. The curves show the counts per minute recorded in each analyzer channel plotted against the channel number, indicated at the bottom, and against the approximate energy given up within the sensitive volume of the chamber, indicated at the top. (The relationship between channel number and pulse energy is

FIGURE 1

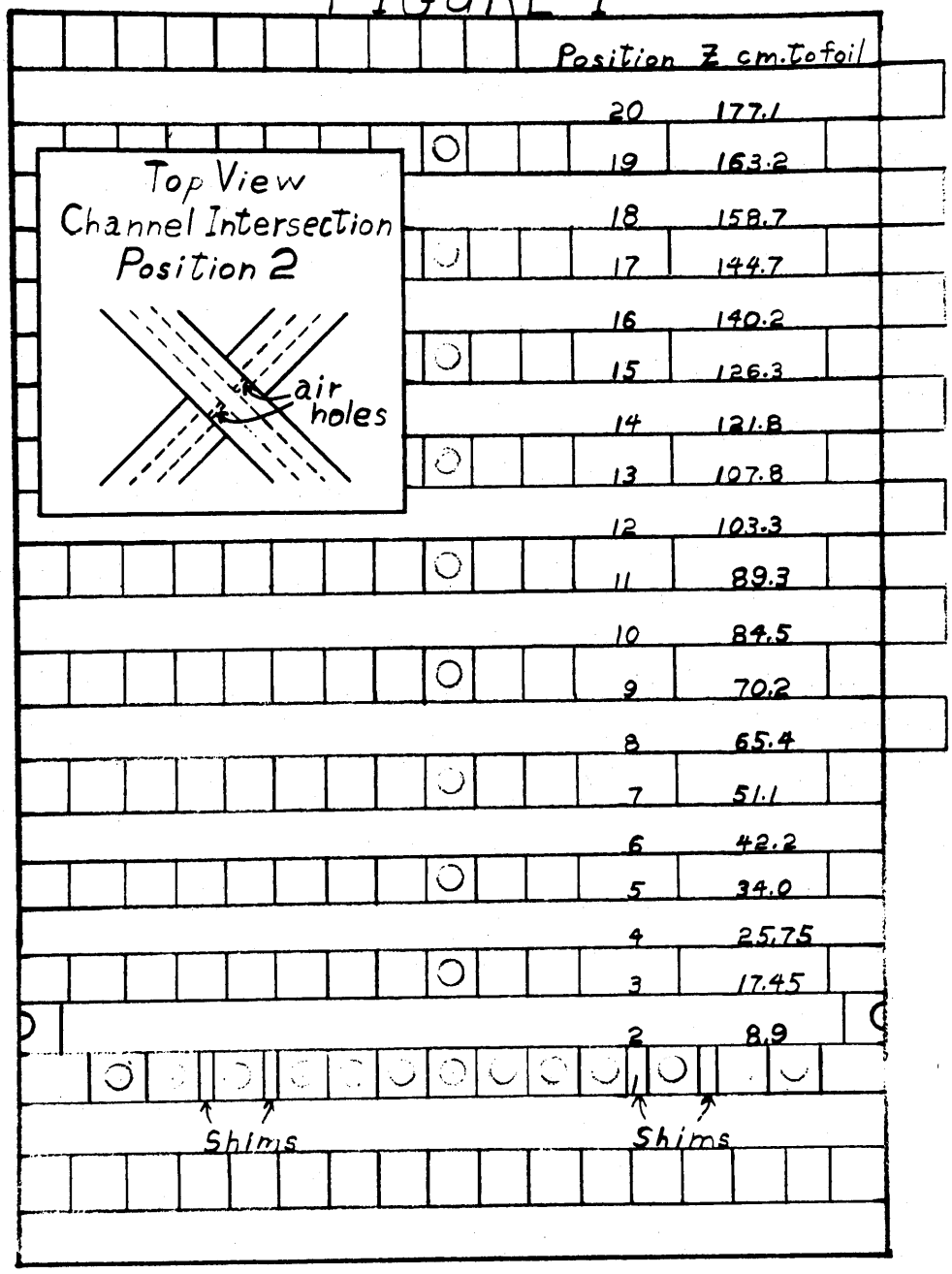


North Face
Scale: 1"=10"

FIG. 8 GRAPHITE STANDARD PILE
(FROM REFERENCE 20)

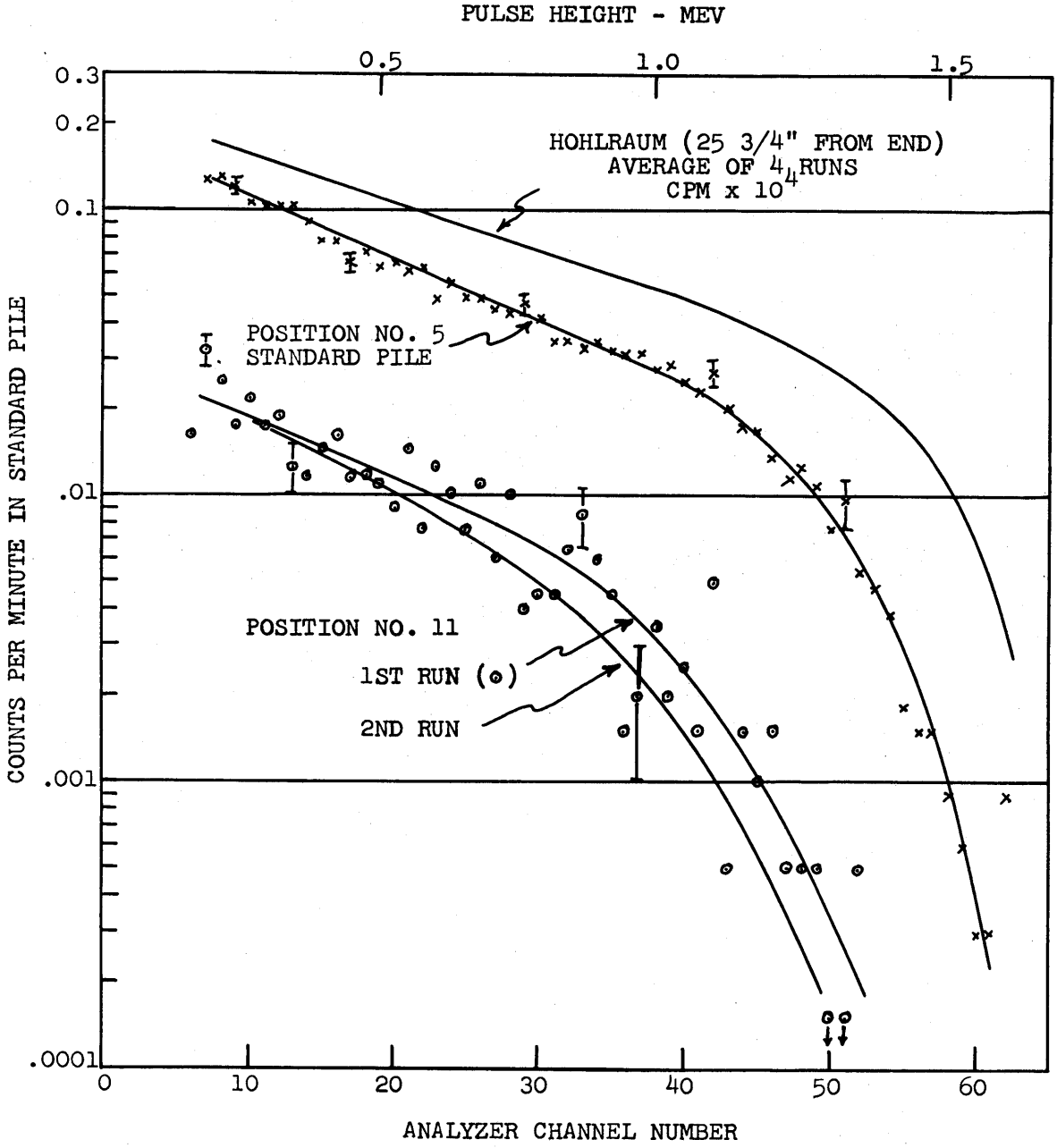


FIG. 9 COUNTER NO. 4 (WITH STANDARD B-2a) CALIBRATION RUNS IN STANDARD PILE (JULY 1963). AVERAGE OF 4 HOHLRAUM RUNS FOR COMPARISON.

discussed below in the next subsection.)

For comparison with the curves of the standard pile runs, the average of four runs made in the hohlraum, with the same counter and standard, is also shown.

The run in Position No. 5 and both runs in Position No. 11, together with the corresponding count rates obtained on the Model 132 scaler, have all been used to determine the neutron flux in the pile oscillator tube in the reactor. At the usual operating position (25 3/4" back from the inner end of the tube) the thermal neutron flux is calculated to be $1.14 \pm 0.18) \times 10^8$ neutrons/$cm^2$-sec. At a point 1 3/4" back from the inner end of the tube (due to the length of the detector, this represents the innermost position for which the flux could be measured) the flux was found to be $(1.71 \pm 0.27) \times 10^9$ neutrons/$cm^2$-sec. These flux values and others along the tube are plotted in Figure 10. For comparison with the flux curve, the graphite and shielding configurations at the end of the hohlraum are sketched on the graph. The reason for selecting 25 3/4" as the usual operating position will be discussed below in Subsection C.

C. Counter Characteristics

A typical characteristic curve of alpha counting rate as a function of operating voltage is shown in Figure 11. A-$CO_2$ and A-$CH_4$ were both run to confirm the fact that there should be no significant differences in the counter performance. (A-$CH_4$ is used later to investigate the effect on count rate of recoil nuclei caused by fast neutrons.) An operating voltage of 1400 volts was employed for normal operation.

Figure 12 illustrates the effect on counting rate of diameter of the spherical tip used to cover the sharp end of the anode wire. A diameter of 0.052"was selected for general use.

A characteristic curve for 100% carbon dioxide is shown in Figure 13. Since a much higher anode voltage, about 2400 volts, is required, insulation breakdowns were frequently experienced, and this gas was not used.

No accurate method was available for calibrating the

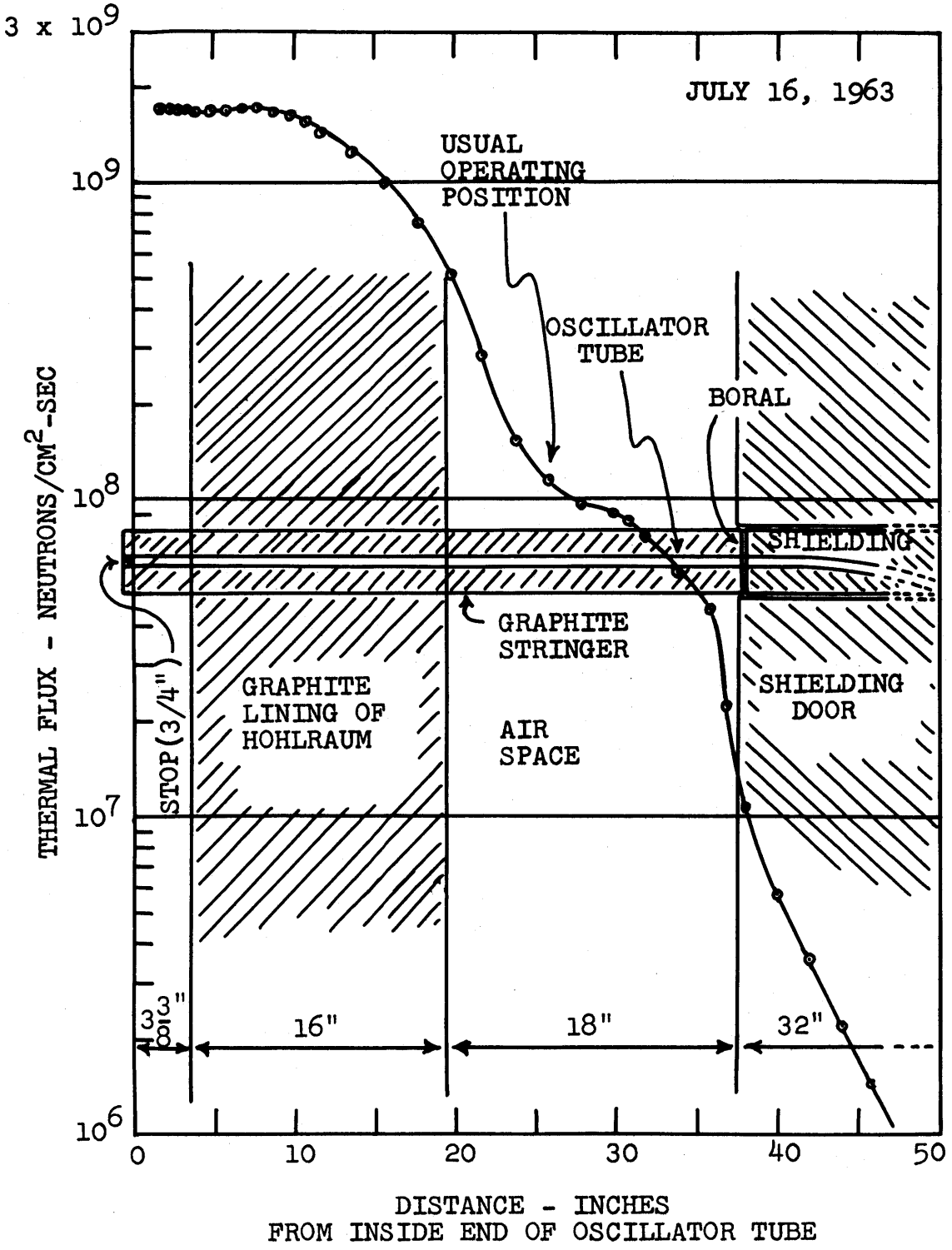


FIG. 10 THERMAL FLUX MEASURED IN PILE OSCILLATOR TUBE AND GRAPHITE CONFIGURATION AT END OF HOHLRAUM (REACTOR POWER 1.95 MW)

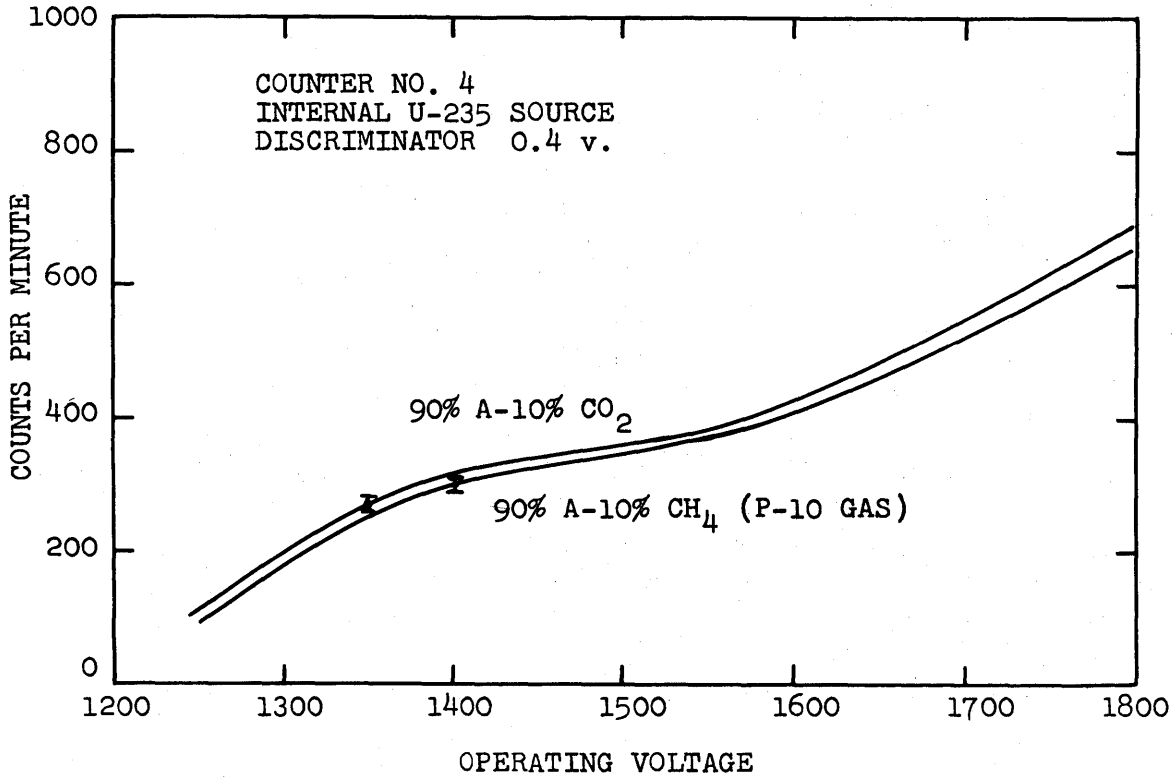


FIG. 11 CHARACTERISTIC CURVES OF ALPHA COUNTING RATE VS. OPERATING VOLTAGE FOR TWO COUNTING GASES. (TMC ANALYZER NOT ATTACHED) (JULY 10, 1963)

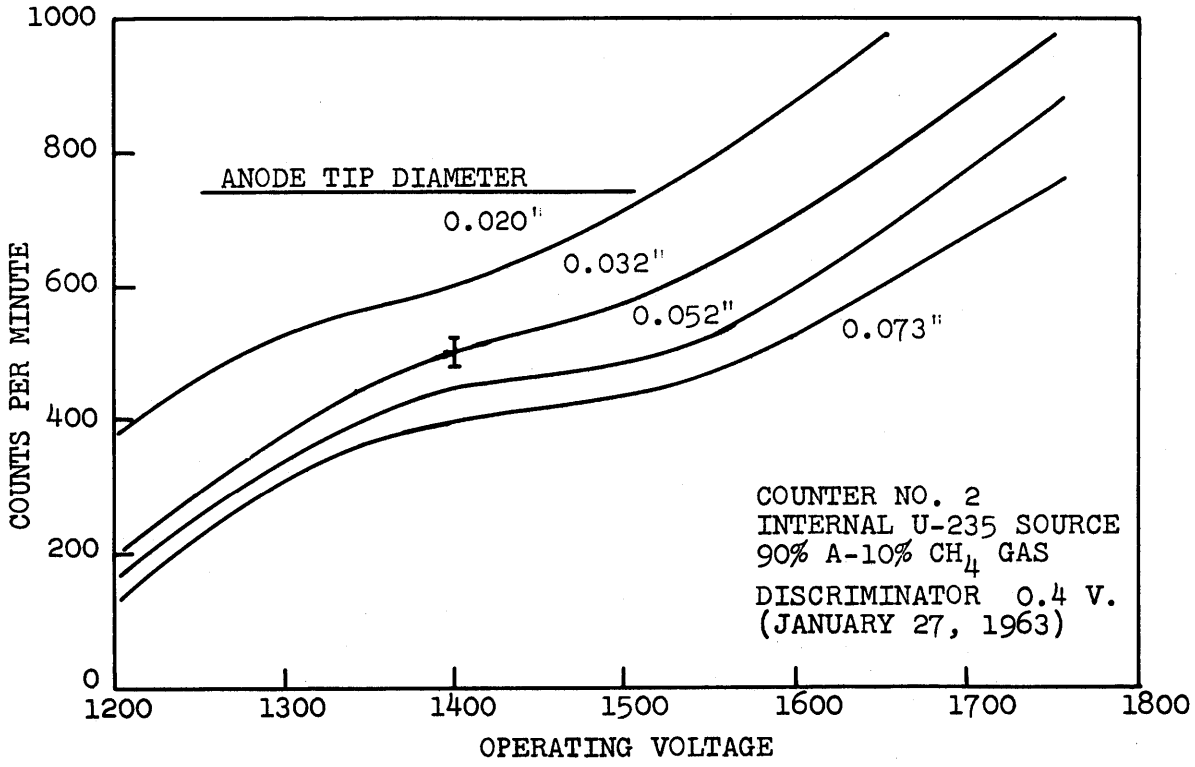


FIG. 12 EFFECT OF DIAMETER OF ANODE TIP ON CHARACTERISTIC CURVE

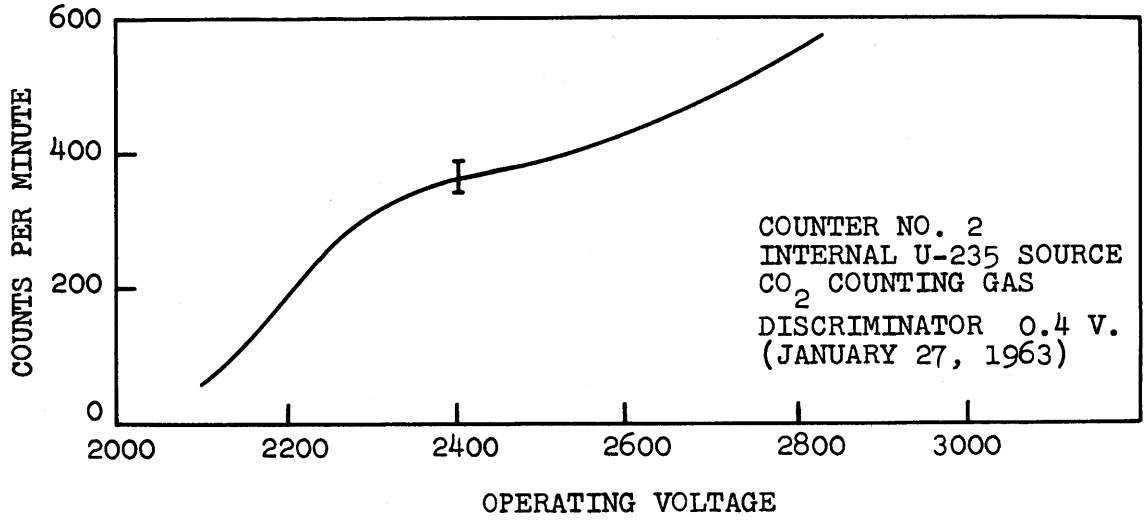


FIG. 13 CHARACTERISTIC CURVE FOR CARBON DIOXIDE COUNTING GAS

multichannel analyzer with respect to the energy given up by a particle passing into or through the chamber. Only a rough calibration was possible, based on a combination of experimental results.

Some useful information was gained by measuring the energy spectrum of the alpha particles emitted by the internal uranium-235 source used for the characteristic curve runs. These energy spectra were measured on several occasions, ostensibly under similar conditions, and yet significantly different results were obtained on each of five runs. Figure 14 presents these results. There seems to be no ready explanation for the apparently chronological progression of the peak, and of the entire curve, toward higher channel numbers. It is possible that there may have been a gradual change in the configuration of the source itself, of the anode position, of the overall system gain, or of some other parameter. Additional investigation would be helpful here.

Immediately after the July 11, 1963, measurement of the alpha spectrum with 90% A-10% $CO_2$, the counting gas was changed to 90% A-10% $CH_4$, and another run was made for comparison. The results are shown in Figure 15, the A-$CO_2$ curve being a repeat of that in Figure 14. There is some question concerning the validity of the differences in these curves, because the A-$CH_4$ plot is quite similar to the average of the A-$CO_2$ curves of the preceding graph. It was not believed important, from the point of view of this activation analysis work, to investigate this question further.

The above energy spectra for the uranium-235 source, with A-$CO_2$ gas, provide one basis for the energy calibration of the multi-channel analyzer. The energy spectra measured for the boron and lithium standards, to be discussed later, also provide a basis for an energy calibration. The overall average of the data utilized for this purpose is 0.026 Mev/channel with a standard error on the order of 0.005 Mev/channel. This was the calibration used for determining the energy scale at the top of all the analyzer energy-spectrum graphs.

It was important to know how ionizing events which occur

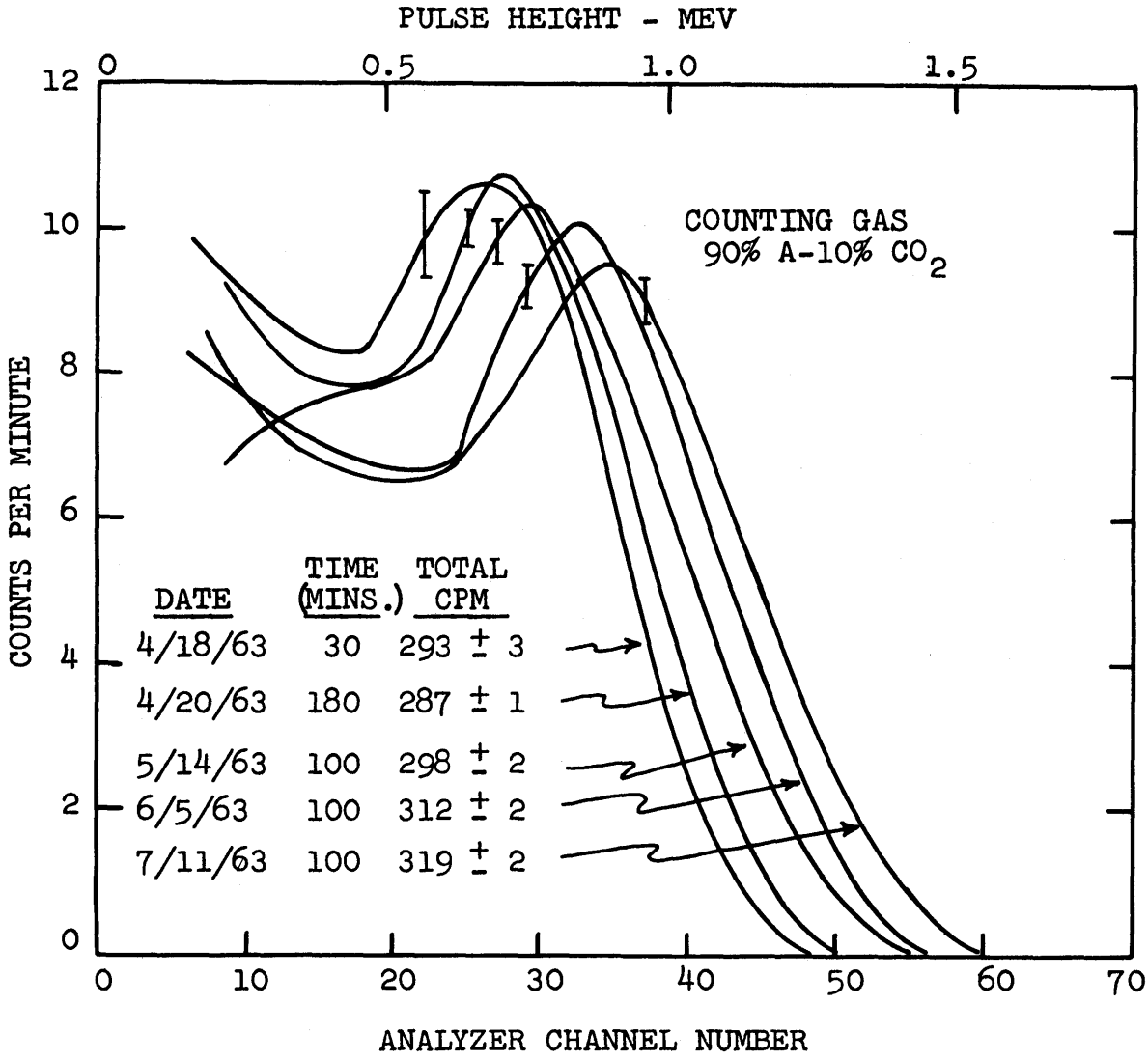


FIG. 14 DISTRIBUTION OF ENERGIES LOST BY ALPHA PARTICLES FROM U-235 SOURCE WITHIN DETECTOR. FIVE RUNS UNDER APPARENTLY SIMILAR CONDITIONS.

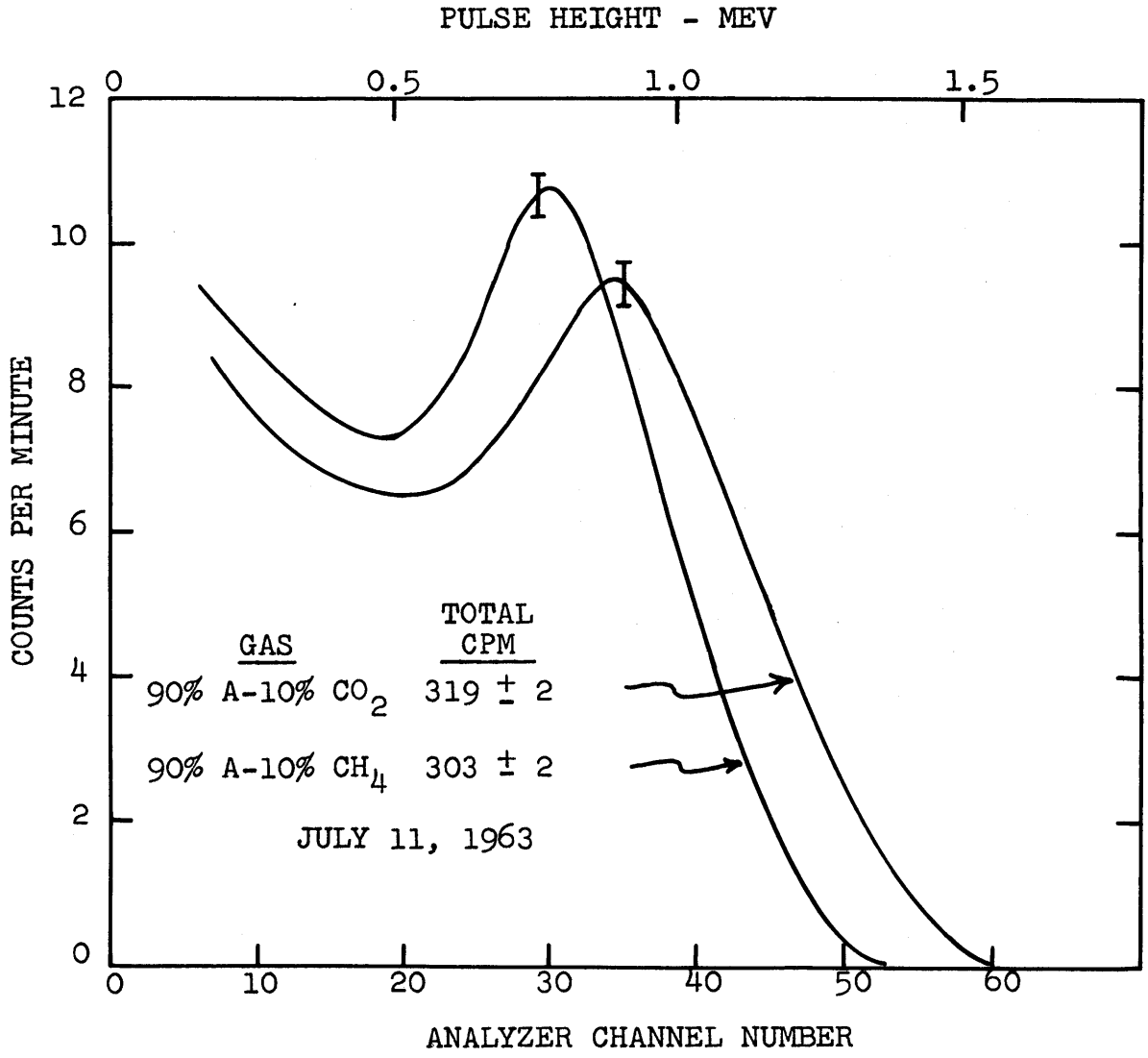


FIG. 15 EFFECT OF DIFFERENT COUNTING GASES ON DISTRIBUTION OF ENERGIES LOST BY ALPHA PARTICLES FROM U-235 SOURCE WITHIN DETECTOR

in the detector, whether or not large enough to be recorded as counts, might affect the performance. For instance, for pluses large enough to be recorded, the observed count rate may be less than the true count rate due to resolving time losses. Also, the creation, even by pulses too small to be counted, of many ion pairs per unit time may result in a space charge if the positive ions did not migrate quickly enough away from the anode wire. The consequent reduction in gas amplification alters the energy spectrum and reduces the count rate.

Runs were first made at a number of positions in the oscillator tube, and the resulting energy spectra were compared to see if the count rates changed proportionately in all channels as the counter position and flux level varied. By plotting the results on semi-log graph paper, it was a simple matter to compare the curves and to see if the shapes were the same, merely displaced from each other by constant amounts in all channels.

Some of the spectrum data taken during the calibration run for the oscillator tube are plotted in Figure 16. These curves illustrate the distortion which occurs at the higher count rates. The slopes of the top curves are slightly greater than those at the lower flux levels, but most obvious is the rapid decrease in count rate in the high channel numbers for flux levels above $10^8$ neutrons/$cm^2$-sec. These curves were made with the aluminum standard containing 290 ppm boron, so that high count rates for alpha and $Li^7$ pulses were obtained (613,620 CPM, corrected). The effect of space charge on gas amplification is especially apparent in the reduction of pulse height and, consequently, channel number for the top two curves. There is little change in the shape of the curve for fluxes below $10^8$ neutrons/$cm^2$-sec.

It is conceivable that the different shapes for the curves of Figure 16 might not be a function of counting rate but rather might be due to a change in the radiation spectrum (both neutrons and gammas) as the counter was moved from the hohlraum, into the graphite wall, and then into the region

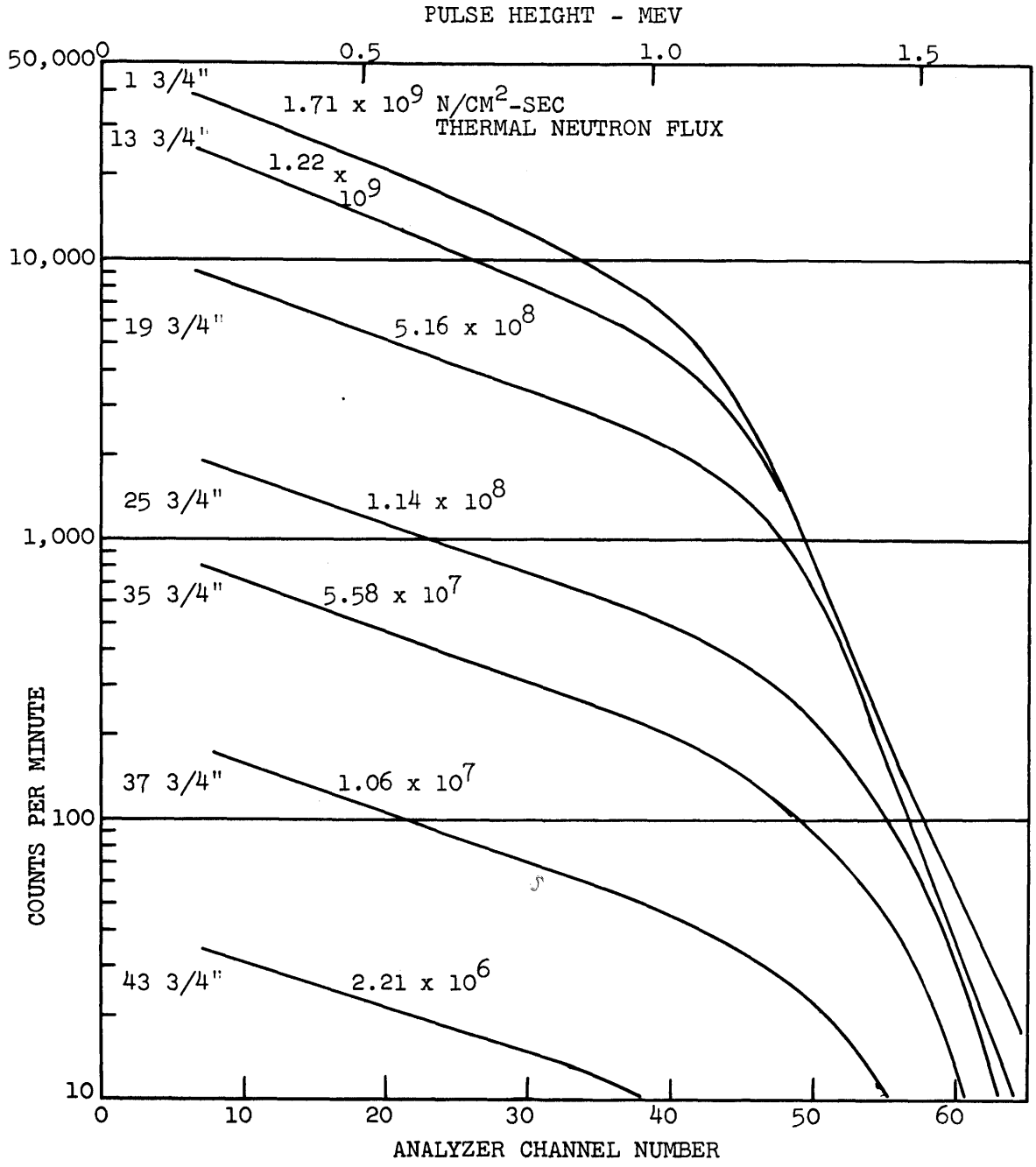


FIG. 16 ENERGY SPECTRA FOR CALIBRATION RUN IN PILE OSCILLATOR TUBE (12 CHI) USING ALUMINUM STANDARD B-2a (290 PPM BORON) (JULY 16, 1963)

between the wall and the shielding.

In an effort to determine the magnitude of the counting error which might be introduced by the distortion of the energy spectrum and also to see if the same distortion would occur if the counter were operated in a single position but at different flux levels, a run was made with the counter located at the inner end of the tube, and the flux was varied by having the reactor reduce power in a series of steps. The same counter and aluminum standard (290 ppm boron) were used as in the runs for Figure 16. Although the decay gammas from the reactor core would prevent the radiation spectrum from being entirely proportional to reactor power, this run had the advantage of eliminating any effect which might result from a change in position.

The results of the run are plotted in Figure 17. It is apparent that the same distortion occurs for the higher count rates. The fact that the lower curves of Figure 17 extend to higher channel numbers before dropping off sharply, in contrast to the upper curves of Figure 16, which were run at the same position, eliminates change in position as being responsible for the change in shape. It now appears likely that counting rate, or at least ionization rate in the chamber, is responsible for the distortion.

It will be noted that the flux level for the top curve of Figure 17 is only $8.42 \times 10^8$ neutrons/$cm^2$-sec., as compared to a flux of $1.71 \times 10^9$ neutrons/$cm^2$-sec. measured for the innermost position of the oscillator tube during the calibration run. It was learned after the run made with reduced reactor powers that the cadmium shutter on the reactor thermal column had closed about half way as the result of a faulty operating mechanism. The corrected count rates indicate that the flux level at full power (2000 KW) was only 49.2% of the level obtained with the shutters fully open. As discussed above, the energy spectrum distortion for the upper curves was evident even with the reduced flux levels.

Because of the distortion resulting from the higher fluxes, the counter was generally operated at a position where the

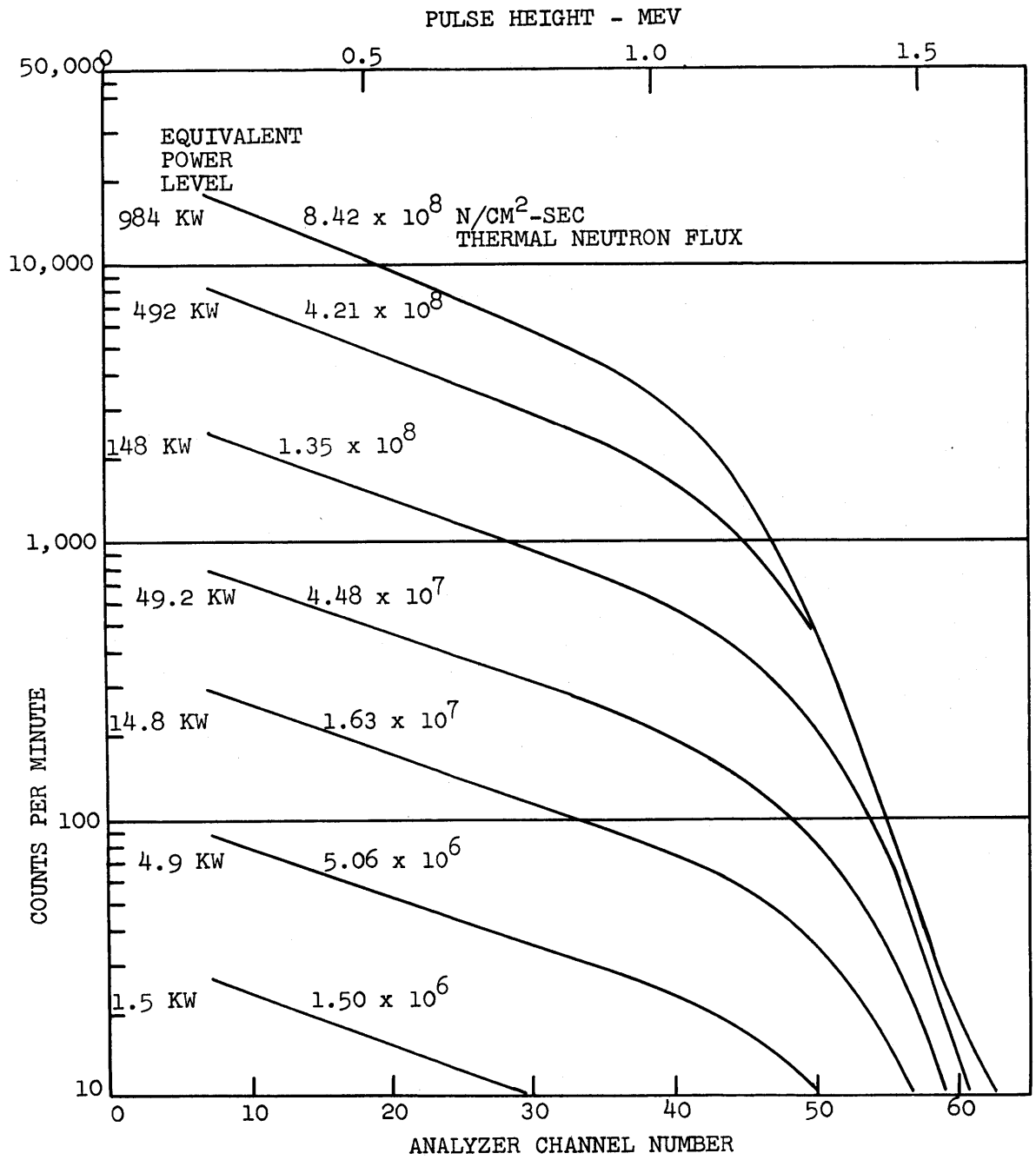


FIG. 17 EFFECT OF FLUX LEVEL ON SHAPE OF ENERGY SPECTRUM FOR ALUMINUM STANDARD B-2a (290 PPM BORON) (JULY 11, 1963)

center of the chamber was 25 3/4" from the inside end of the oscillator tube (24" back from the innermost operating position for the counter). As indicated in Figures 10 and 16, the flux at this point was 1.14 ($\pm$ 0.18) x $10^8$ neutrons/$cm^2$-sec. As may be seen from Figure 10, this position lies between the shielding and the 16" graphite lining for the back of the hohlraum. In general, this region is an 18" air space, but the oscillator tube itself lies within a 4" x 4" graphite stringer reaching from the shielding to the end of the tube. For all of the aluminum standards containing boron and lithium, the counting rates were high enough (a low of 587 CPM for 5 ppm boron) to provide good counting statistics in a reasonable length of time, 1-20 minutes.

On the subject of space charge in the detector, the magnitude of the effect will depend upon the number of ion pairs created per unit time and not necessarily on the count rate. Figure 18 is an example of spectrum distortion occurring at count rates as low as 2,143 CPM, as compared to 613,620 CPM for the 290 ppm boron standard. Spectra and count rates were taken for both cases while the detector was operating at the innermost position in a flux of 1.71 x $10^9$ neutrons/$cm^2$-sec. In the former case, the sample was No. S-b (99.9999% Al) with less than 1 ppm boron plus lithium. Even with its comparatively low count rate, the spectrum of Sample No. S-b drops off faster in a flux of 1.71 x $10^9$ neutrons/$cm^2$-sec than it does in a flux of 1.14 x $10^8$. As may be seen in Figure 18, the same is true of a sample of reactor-grade graphite, Gr-b, for which the counting rate was only 4,715 CPM at the higher flux. An even more striking example is shown in Figure 19, in which are plotted the energy spectra for a gold sample operated at the above two flux levels.

Even though the pure aluminum and graphite samples show irregularities in the energy spectra which are not apparent in the aluminum standards containing higher amounts of boron or lithium, nevertheless, the effects of space charge are clearly evident. The high ionization necessary to produce this space charge can be explained, in the absence of a high

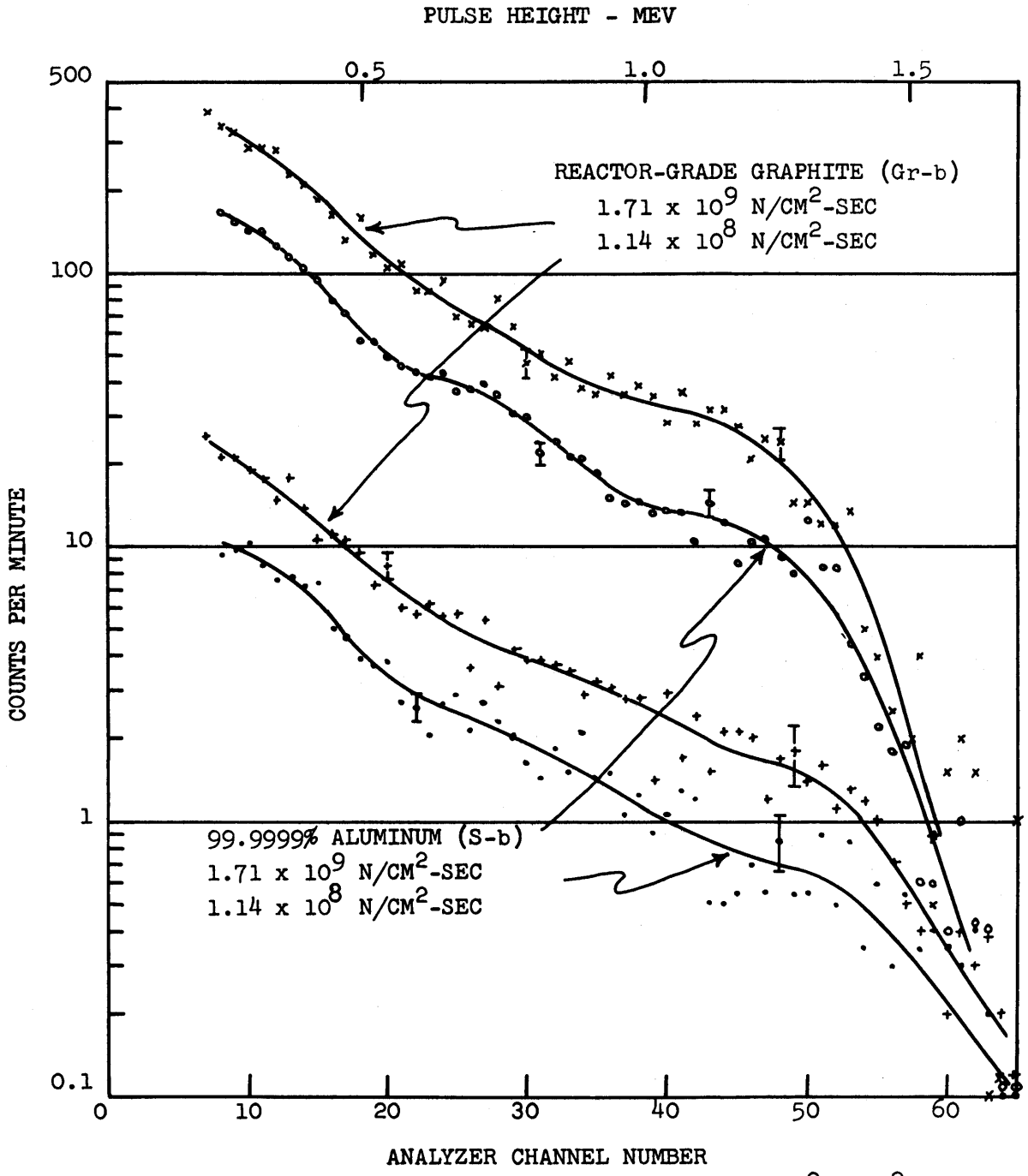


FIG. 18 DISTORTION OF ENERGY SPECTRA AT $1.71 \times 10^9$ N/CM$^2$-SEC DUE TO SPACE CHARGE (MAY 6-7, 1963).

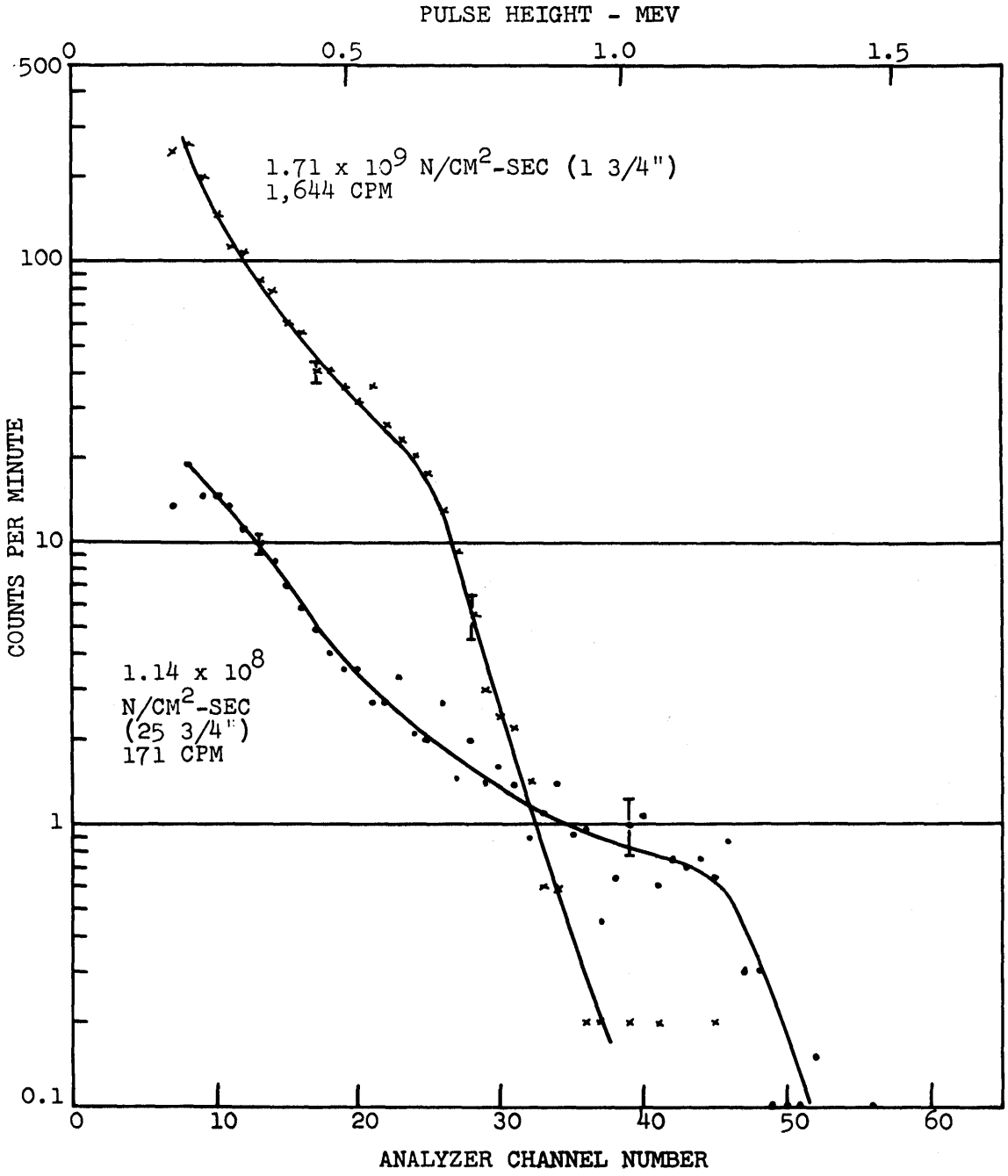


FIG. 19 DISTORTION OF ENERGY SPECTRUM FOR GOLD AT 1.71 x $10^9$ N/$CM^2$-SEC DUE TO SPACE CHARGE (APRIL 24, 1963)

alpha count rate, by the fact that photoelectrons and Compton recoils (and pair production) from gamma radiation create a very high electron flux in the detector, particularly for the operating positions near the inner end of the oscillator tube. In addition, decay betas from the aluminum parts of the detector constitute a further source of ionization within the counter.

The densities of electron and beta pulses for various counter positions are shown in Figures 20a, b, and c. The high density for the usual operating position (25 3/4") is an indication that there must be many multiple coincidences for the innermost position, Figure 20c. If $10^5$ large electron and beta pulses per second is considered to be a conservative minimum at the 25 3/4" position, the rate for the innermost position appears to be well in excess of $10^6$ pulses per second. Since the maximum count rate for the 290 ppm boron standard was about $10^4$ CPS (613,620 CPM) and since the largest electron pulses were roughly $1/50^{th}$ the size of the largest alpha pulses, the ionization due to the electrons and betas is seen to be at least double the ionization due to the alphas. When the resulting space charge is large enough, the pulse heights of the heavy particles are reduced, and a distortion of the energy spectrum occurs.

A photograph of typical alpha pulses is shown for comparison in Figure 20d. (The position of the trace was raised so that the sweep to the right of the pulses would be partly cut off by the top deflection plate of the cathode ray tube, thereby reducing the intensity in that region enough to permit photographing. This did not alter the appearance of the trace.)

There were times when small changes in counting rates were noted during consecutive runs under similar conditions, and it was thought that an increasing flux of decay betas from aluminum in the detector might be the cause of the change. This possibility was investigated by rapidly inserting the counter, with the 290 ppm boron standard, into the innermost position (highest flux). A series of 0.10-minute counts and

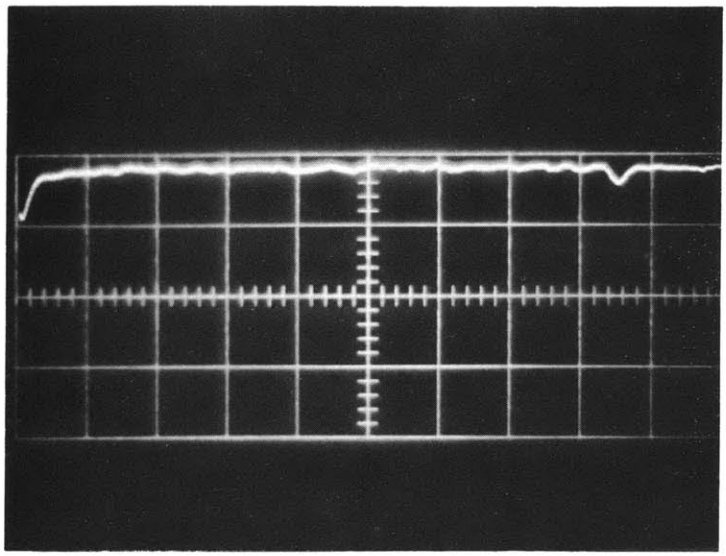

FIG. 20a ELECTRON PULSES OBSERVED IN 99.9999% ALUMINUM SAMPLE, S-b.
FLUX(at 46 3/4") 1.13 x $10^6$ NEUTRONS/$CM^2$-SEC
HORIZONTAL SWEEP: 10 μs/cm.
VERTICAL DEFLECTION: 0.01 v/cm.

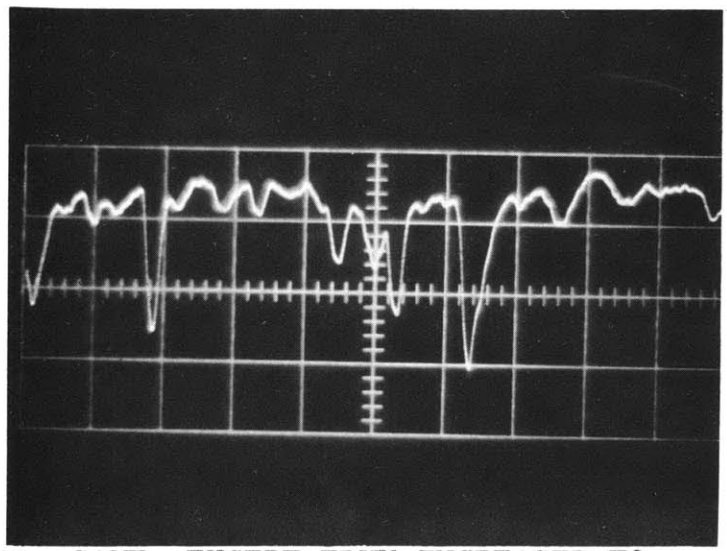

FIG. 20b SAME, EXCEPT FLUX INCREASED TO 1.14 x $10^8$ NEUTRONS/$CM^2$-SEC (USUAL OPERATING POSITION, 25 3/4")

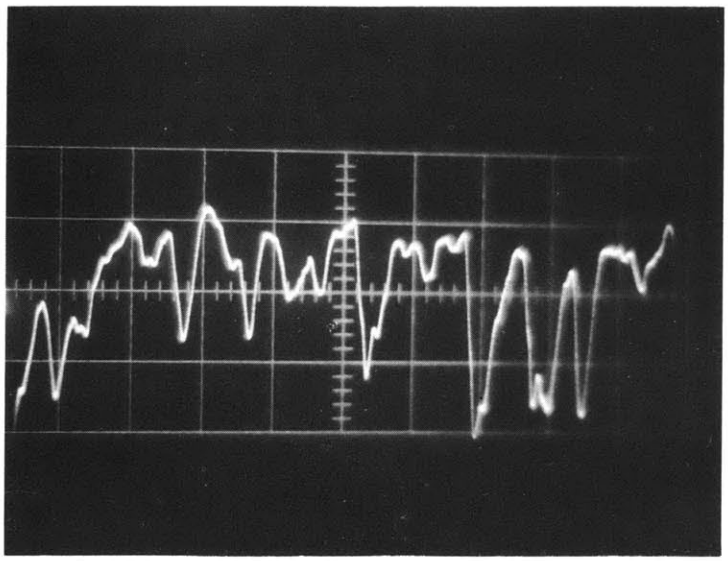

FIG. 20c SAME AS FIGURE 20a, EXCEPT FLUX INCREASED TO $1.71 \times 10^9$ NEUTRONS/$CM^2$-SEC (INNERMOST OPERATING POSITION, 1 3/4")

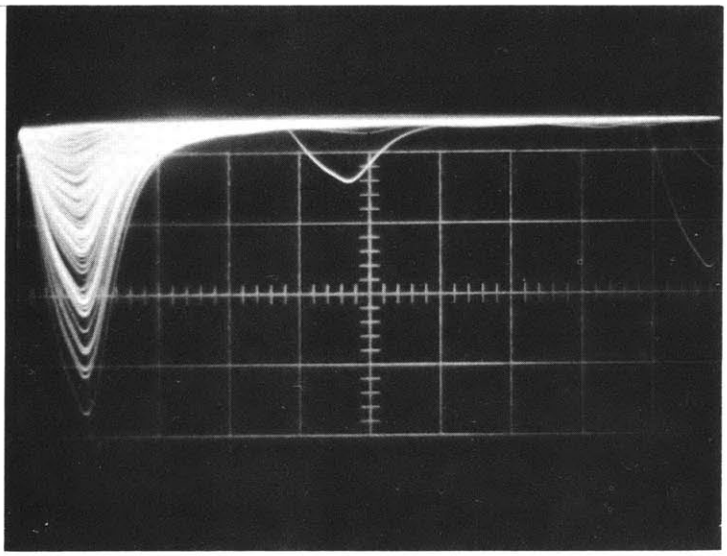

FIG. 20d ALPHA PULSES OBSERVED IN ALUMINUM STANDARD B-2a (290 ppm BORON)
FLUX (at 25 3/4"): $1.14 \times 10^8$ NEUTRONS/$CM^2$-SEC
HORIZONTAL SWEEP: 2 μs/cm.
VERTICAL DEFLECTION: 0.2 v/cm.

observations of the energy spectra were then made over a 14-minute interval while the activity of the aluminum-28 (half life 2.3 minutes) was building up to saturation. The single curve of Figure 21 represents three 0.10-minute runs made (1) immediately after insertion, (2) two minutes after insertion, and (3) 14 minutes after insertion. The results of all three runs were identical, indicating that the contribution of the aluminum-28 decay betas to the space charge effect is not important.

It was pointed out earlier in this subsection that the effect of space charge on the pulse height might reduce the accuracy of the observed count rates. Since the "live time" feature of the TMC analyzer cannot compensate for this type of error, it was felt necessary to determine the magnitude of any error which might result from the space charge effect.

Data from the runs discussed above were further analyzed to determine the magnitude of errors in the observed counting rates. This was done for the Model 132 Scaler as well as for the TMC Analyzer. The calculations show that the count rates observed on the scaler must be increased to compensate for an average dead time of $0.317 \times 10^{-6}$ seconds/count. This requires a 14.6% increase in the observed count rate of 397,900 CPM in order to obtain the true count rate of 458,950 CPM for the 290 ppm boron standard operating in the highest flux.

In the case of the TMC Analyzer, it would be expected that the "live time" feature would compensate for system dead time, but also that the effect of space charge would reduce the observed count rate to a figure somewhat below the true count rate. However, the calculations show that the observed count rate is higher than the true count rate, so that a "live time" correction, calculated to be approximately $0.283 \times 10^{-6}$ seconds/count, must be applied to the observed rates but in a direction opposite to that of the usual dead-time correction. This error more than compensates for any loss in counts which might result from the reduction in pulse height due to space charge. At the maximum observed count

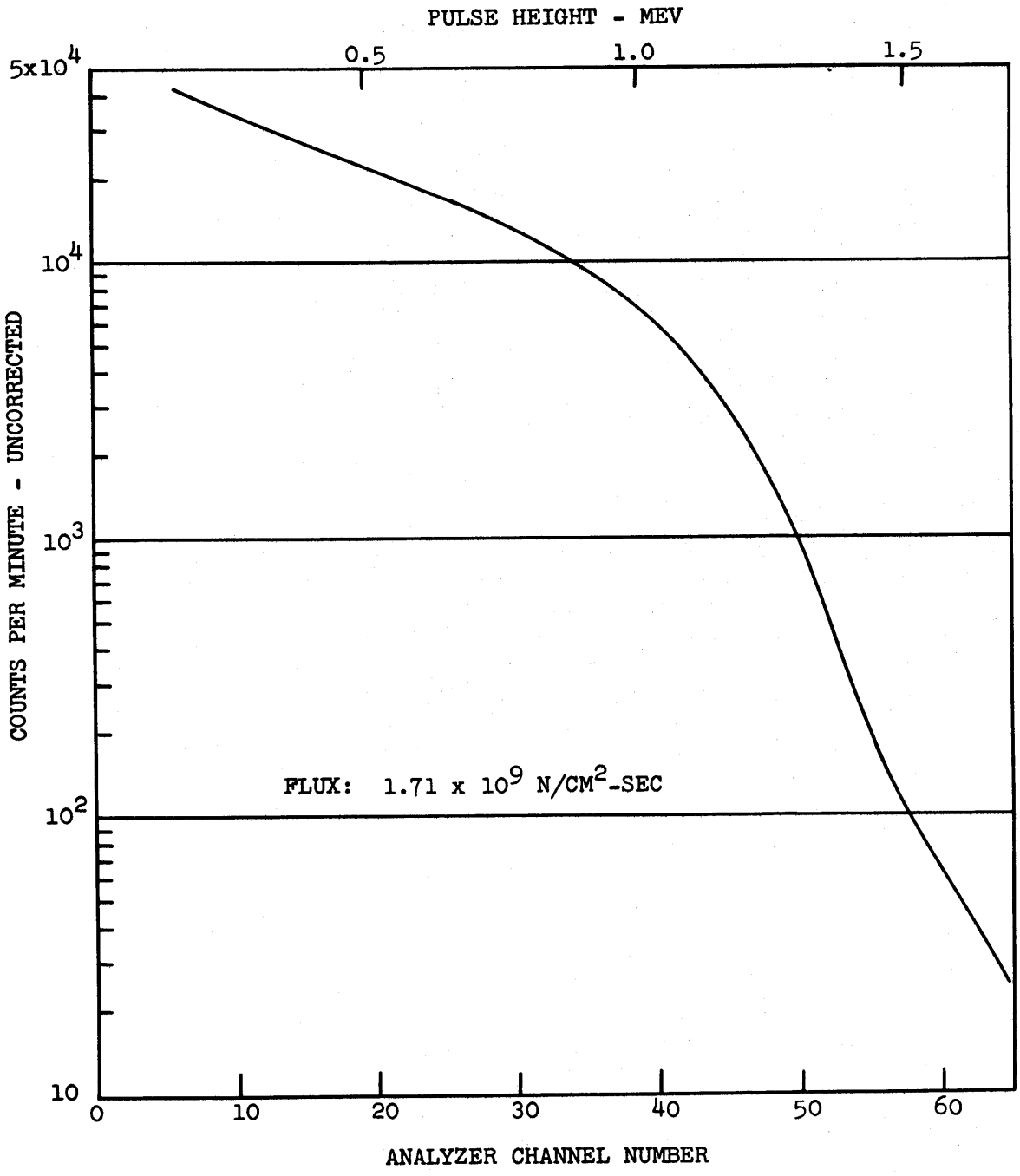


FIG. 21 EFFECT OF ALUMINUM-28 DECAY BETAS ON ENERGY SPECTRUM OF ALUMINUM STANDARD B-2a (290 ppm BORON) (JULY 16, 1963)

rate of 743,120 CPM, a 17.5% correction is required, which reduces the value to 613,620 CPM. At the usual operating position (25 3/4"), the "live time" corrections do not exceed 1%, and therefore, no corrections have been applied to the TMC data taken at that point. For TMC data involving count rates higher than those measured at 25 3/4", such as the pile oscillator tube flux calibration, the "live time" correction factor has been applied.

Selection of the point at 25 3/4" from the inner end of the tube as the usual operating position had not only the advantage that corrections to the observed count rates could be neglected but also the favorable aspect that the slope of the flux curve is somewhat flatter than it is in adjacent regions of higher flux.

## D. Results of Measurements on Aluminum Standards

In general, as mentioned earlier, the energy spectrum was measured for each of the samples run in the proportional counter during operation in the hohlraum.

For the early runs in the medical therapy room beam, however, only integral bias curves were determined for the samples. The results of such runs are shown in Figure 22 for two aluminum standards containing boron, two aluminum standards containing lithium, an aluminum "blank," and a sample of reactor-grade graphite. Of primary interest are the similarities in the shapes of the boron curves and the distinct differences between the boron and the lithium. These differences led to the use of a multi-channel analyzer in the expectation that the differences would be more pronounced in energy distribution curves than in the integral bias curves. Such was the case, as will be seen below in this subsection.

Other results of interest are the integral bias curves plotted in Figure 23. These runs were made with the boral shutter of the medical therapy beam closed and with the detector enclosed in a 1 1/4" inside diameter sleeve of borated plastic. The double boron shield was intended to reduce thermal neutrons practically to zero in an effort to bring out the effects, if

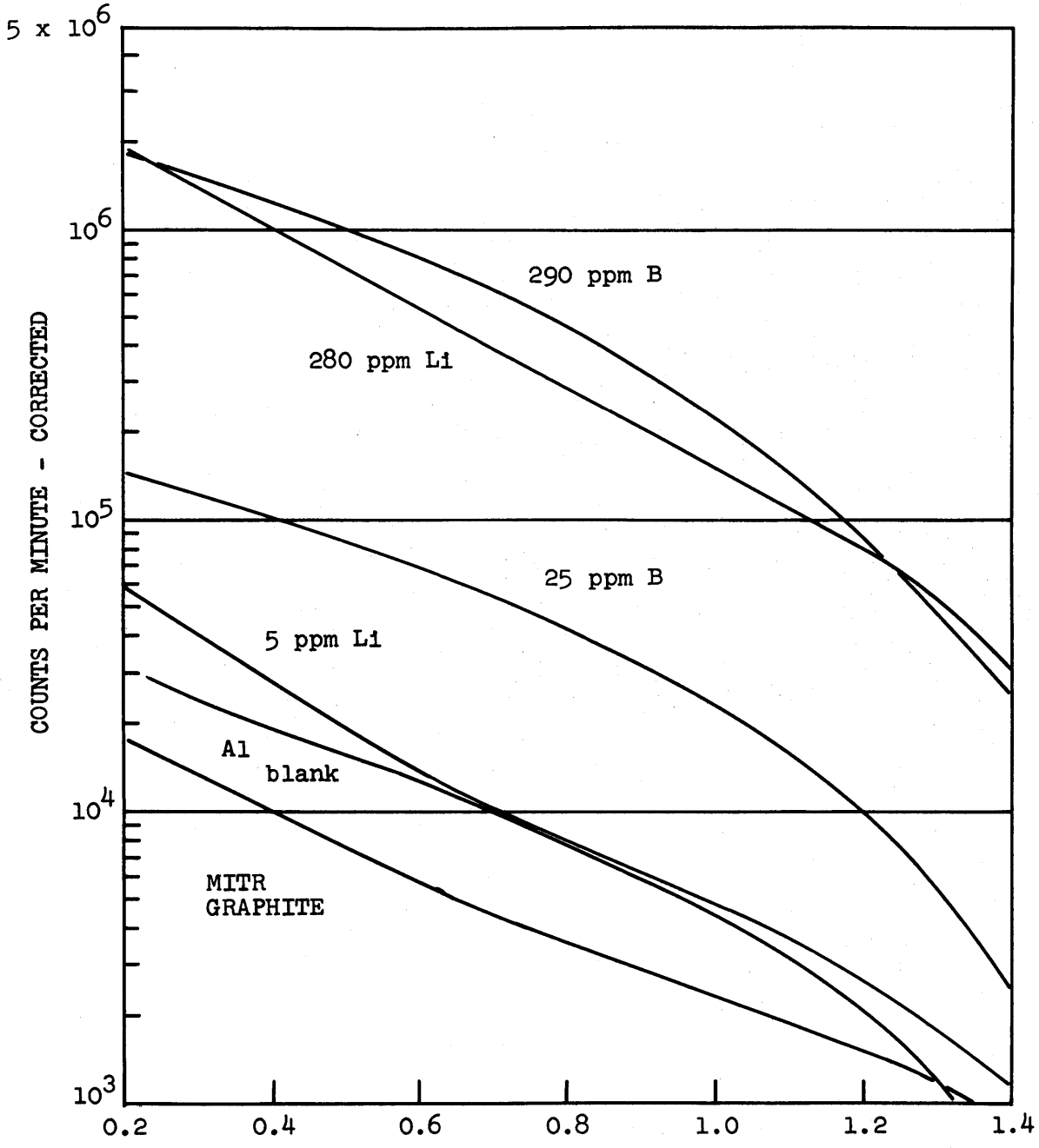


FIG. 22 INTEGRAL BIAS CURVES FOR SAMPLES RUN IN MITR MEDICAL THERAPY ROOM (FEBRUARY 12-13, 1963)

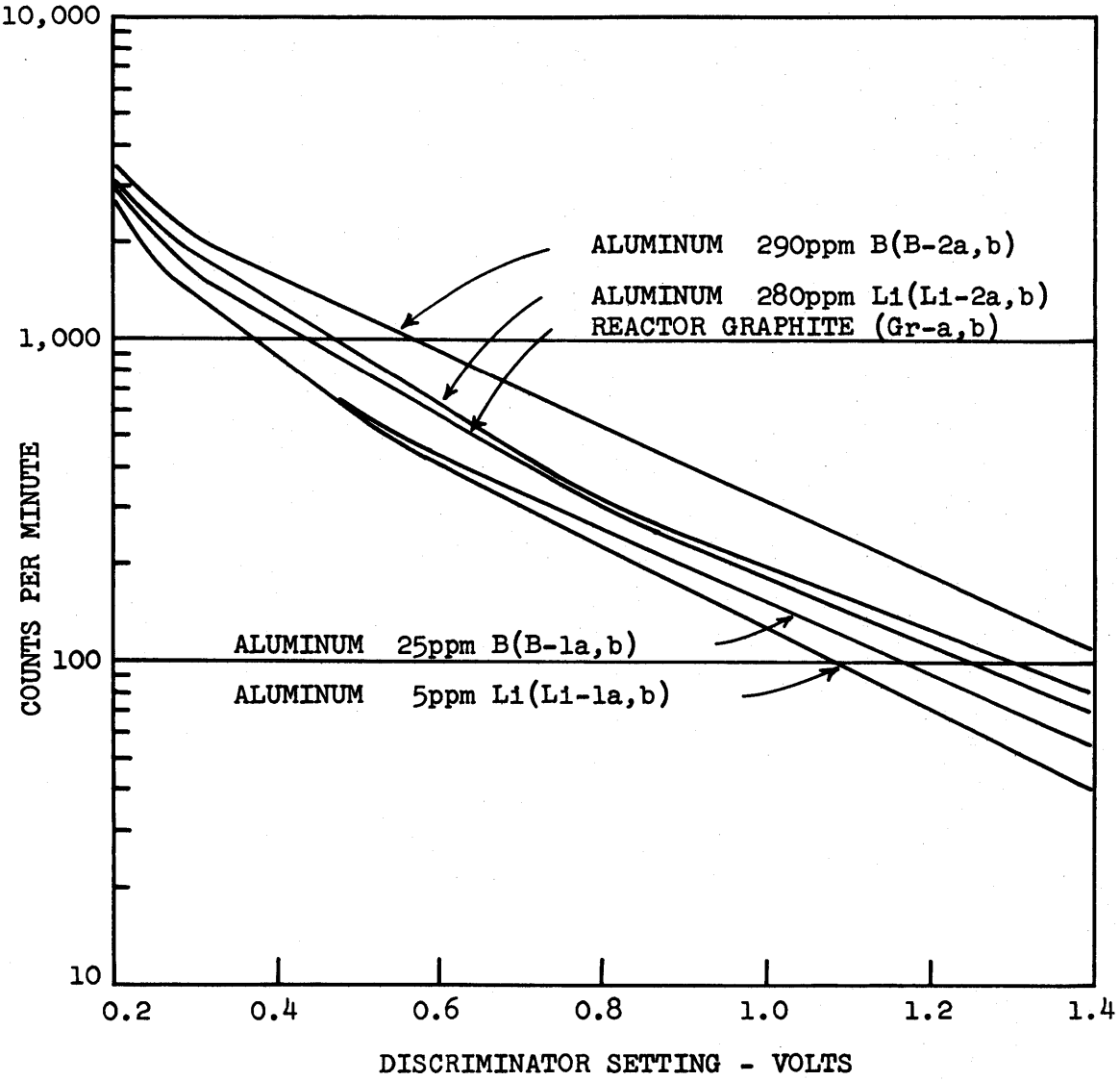


FIG. 23 INTEGRAL BIAS CURVES FOR SAMPLES IN FAST NEUTRON FLUX OF MEDICAL THERAPY ROOM (FEBRUARY 12, 1963)

any, of fast neutrons. It is believed that such an effect is evident because these curves differ substantially from the previous curves of Figure 22, which were run without any neutron shields. In addition to having count rates several orders of magnitude less than those of the unshielded runs, the second set of curves shows the following differences:

1) The ratio of count rates for the 290 ppm boron to those for the 25 ppm boron is about two instead of 10-12. The same reduction in count rate ratio holds true for the lithium standards. If pulses in the detector were coming only from the thermal neutron reactions, the ratios should be the same in both figures.
2) The curves for the shielded runs are comparatively straight at the higher discriminator settings and do not show a corresponding drop-off at a setting of 1.2 volts.
3) Each curve for the shielded runs shows a distinctly steeper slope in the region of 0.3-0.5 volts discriminator setting than it does at the higher settings.
4) The graphite curve now shows a higher count rate than the aluminum with low concentrations of boron or lithium.

It would be of interest to identify the various factors contributing to the count rates of the shielded runs. Use of a multi-channel analyzer and runs with materials of different atomic weights would help in this respect. For the purposes of this investigation, however, it is sufficient to note that effects probably caused by fast neutrons were evident and that the presence of such effects was confirmation of the desirability of operating in a more nearly thermalized region of the reactor.

All of the runs in the hohlraum were made with the use of a multi-channel analyzer, and the results are presented in the form of pulse energy distribution curves (energy spectra) rather than in the form of integral bias curves.

In this subsection, only the results of runs with the

aluminum standards containing known amounts of boron or lithium are presented, the results for high purity aluminum and graphite samples being given in later subsections. The data is based only on runs made in the "usual operating position" (25 3/4" from the inner end of the pile oscillator tube). The counting rate errors did not exceed 1%, and so corrections have not been made in the observed data.

Energy spectra were determined for 12 aluminum standards containing boron, two samples for each of six boron concentrations. One to four runs were made with each sample, and the total count rates were averaged to obtain the values given in the following table.

TABLE IV-1

SUMMARY OF ALUMINUM STANDARDS WITH BORON

| Analysis (ppm) | No. of Runs | Average (CPM) |
|---|---|---|
| 290 | 4 | 37,829 ± 2,130 |
| 180 | 4 | 23,851 ± 613 |
| 120 | 2 | 14,942 ± 250 |
| 50 | 2 | 7,101 ± 22 |
| 25 | 4 | 2,770 ± 127 |
| 5 | 2 | 587 ± 15 |

The energy spectra for each of the above runs was plotted. An average curve was then drawn for each concentration, and the results are shown in Figure 24.

Primary features of these curves are that they are essentially straight lines up to 1 Mev approximately, the slopes are identical for all except the 5 ppm standard, the shapes are otherwise similar except again for the 5 ppm standard, and the spacing is approximately that which would be expected from

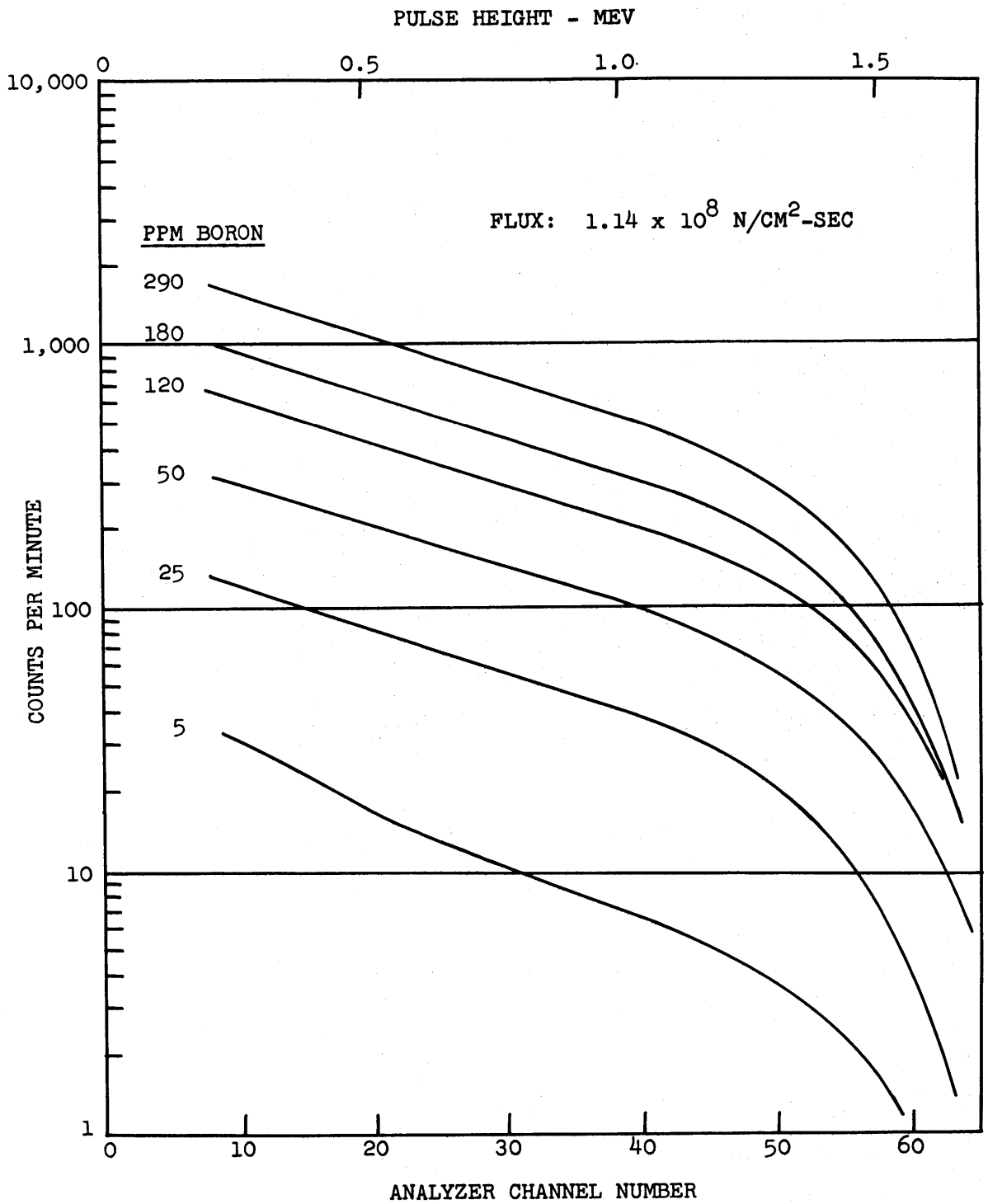


FIG. 24 ENERGY SPECTRA FOR ALUMINUM STANDARDS CONTAINING INDICATED AMOUNTS OF BORON (MAY 14 AND JUNE 6, 1963)

the analyses.

The standard deviations shown in Table IV-1 reflect the count rate variation which was frequently noted from run to run, and which may have been due to slight differences in detector position, operating voltage, hohlraum flux level, surface condition of the sample, etc. In all but one of the 18 runs, the counting time was long enough so that the standard deviation for the run was not greater than 1%, and it was generally much less.

The standard error in the value of the slope is 1% or better, except for the lowest curve, which is approximately 3%.

Based on the estimate, given in Table II-3, of the counting rates for boron in aluminum, the following count rates per square centimeter of effective chamber surface might be expected for the flux level used in these runs, 1.14 ($\pm$ 0.18) x $10^8$ neutrons/$cm^2$-sec.

| Ionizing Particle | Energy (Mev) | CPM/$cm^2$ of surface | |
|---|---|---|---|
| | | 5 ppm B | 290 ppm B |
| $\alpha$ | 1.47 | 434 | 25,200 |
| $Li^7$ | 0.84 | 143 | 8,300 |
| | | 577 | 33,500 |

These values are quite close to the observed count rates but, since the effective surface area of the chamber is probably at least 3 $cm^2$ and since it was assumed in the calculation that every particle entering the chamber would be counted, even though it might have very low energy, it appears that the actual counting efficiencies are only about one third of the assumed values.

7% of the alpha and $Li^7$ particles have energies of 1.78 Mev and 1.01 Mev respectively, a fact which was ignored in the estimate of counting rates for Table II-3 and summarized above. However, these higher energy particles contribute to the shape of the curve, particularly to the maximum energies observed. Indeed, the 1.78 Mev alphas were taken into account

in establishing the energy calibration of the system. In view of the fact that particles of four different energies contribute to the energy spectra, it is probably fortuitous that the curves appear as straight lines up to 1 Mev.

In the case of lithium in aluminum, energy spectra were determined for 10 standards samples, two samples for each of five concentrations. One to three runs were made for each sample, so that two to four usable determinations were available for each concentration. The average count rates are given in the table below.

TABLE IV-2

SUMMARY OF ALUMINUM STANDARDS WITH LITHIUM

| Analysis (ppm) | No. of Runs | Average (CPM) |
|---|---|---|
| 280 | 2 | 46,200 ± 982 |
| 130 | 2 | 22,931 ± 73 |
| 40 | 2 | 7,422 ± 27 |
| 15 | 2 | 2,400 ± 27 |
| 5 | 4 | 1,236 ± 98 |

As for the boron, an average curve was drawn for each set of runs, and the results are shown in Figure 25. It is immediately obvious that the shape of the curves is quite different from those for boron. In particular, the slope of the straight portion of each curve between about 0.3 Mev and 0.8 Mev is much steeper, and there is a fairly sharp bend at about 1 Mev. Above 1.5 Mev, the curves turn downward again and, like the boron, drop quickly to zero. Again, like the boron, the shapes of the curves are identical and the count rates are approximately proportional to the lithium concentration, except for the 5 ppm standard. The magnitude of the experimental errors is comparable to that of the errors for boron.

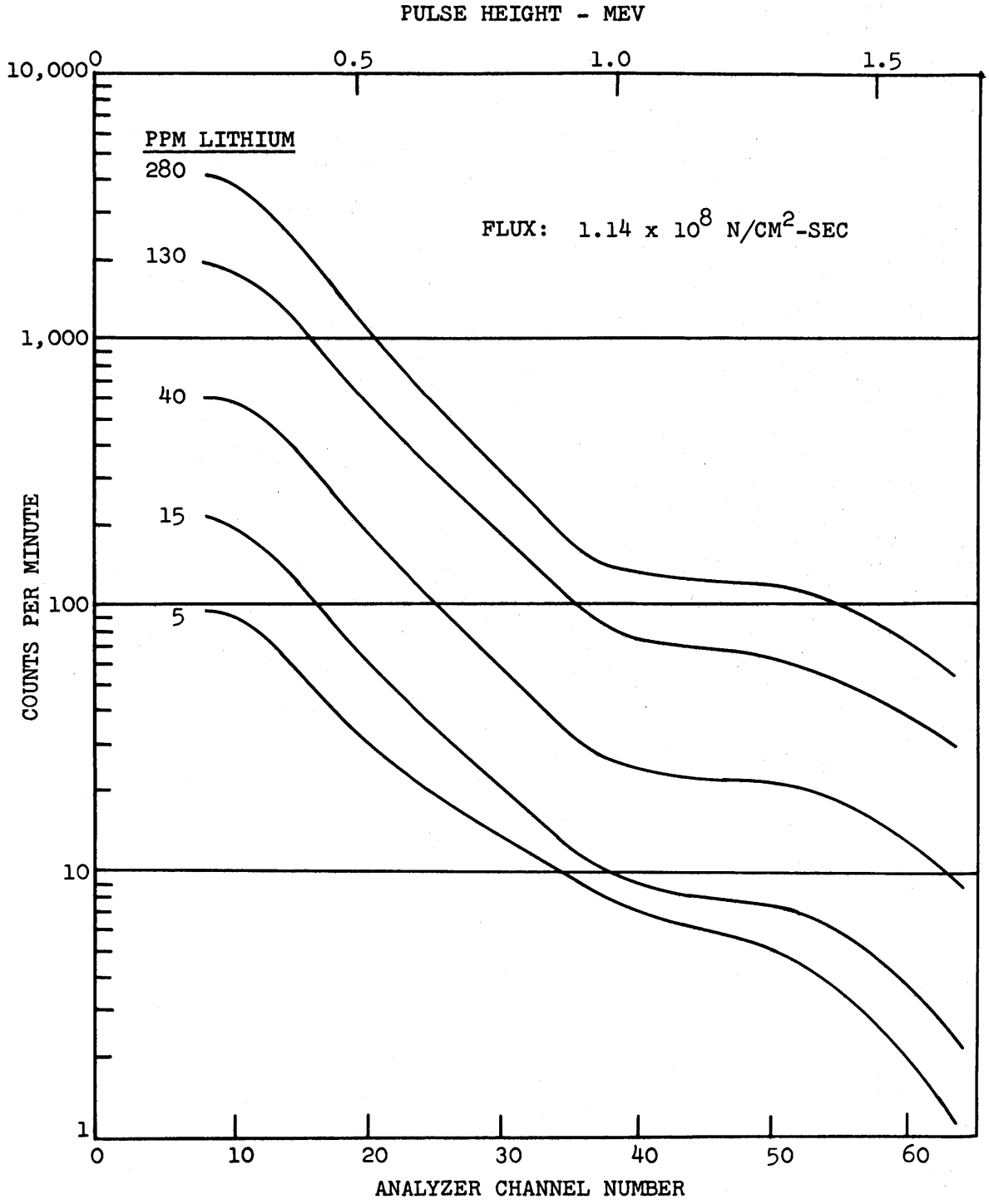


FIG. 25 ENERGY SPECTRA FOR ALUMINUM STANDARDS CONTAINING INDICATED AMOUNTS OF LITHIUM (May 14 and June 6, 1963)

Based on the estimate, given in Table II-3, the following count rates per square centimeter of effective chamber surface might be expected for the flux level used in these runs.

| Ionizing Particle | Energy (MEV) | Range A-$CO_2$(cm) | CPM/$cm^2$ of surface 5 ppm Li | 280 ppm Li |
|---|---|---|---|---|
| $\alpha$ | 2.06 | 1.21 | 91 | 5,100 |
| $H^3$ | 2.73 | 6.98 | 526 | 29,500 |
| | | | 617 | 34,600 |

As for the boron, it appears that the counting efficiencies are about one third of the values assumed for Table II-3.

The shapes of the lithium curves can be explained on the basis of the alpha and triton energies and ranges listed above. The high count rate, low energy portion of the curve is a combination of alpha and triton pulses, primarily the latter. Although the tritons entering the chamber will have energies up to 2.73 Mev, calculation shows that the maximum energy lost in traversing the chamber will be 0.8 - 0.9 Mev. Therefore, the tritons do not contribute to the count rate at the high energy end of the curve. An alpha particle, travelling obliquely across the chamber, could lose all of its energy and give rise to a 2.06 Mev pulse. The TMC was usually operated on one quarter of its memory (64 channels), but extrapolation of the curves does indicate a maximum pulse height of about 2 Mev. It should be pointed out that the channel numbers corresponding to the knee of the lithium curve and to its maximum were two of the four points used to determine an energy calibration for the system.

It is evident that, within the ranges of the standards measured, it should be possible, using the count rate obtained on an aluminum unknown containing only boron or only lithium, to estimate the concentration of whichever element is present. If an energy spectrum curve is determined as well, it should be possible, because of the significant difference between them

for boron and lithium, to distinguish between the two elements and, furthermore, to estimate the ratio in which the two occur.

Figure 26 shows calibration curves for boron in aluminum and for lithium in aluminum. These are based on the standards listed in Tables IV-1 and IV-2, and the errors shown in those tables are indicated for several of the points where they are large enough to plot.

Since the relationship between count rate and concentration is a straight line, it is possible to determine an average figure for the slope of the line in each case. This can be read approximately from the plot for each of the two elements in Figure 26. It is also possible to make a calculation which converts each measurement to a count rate per part per million of boron or of lithium and then weights each such quotient according to its standard error in order to obtain a mean value. These calculations lead to the following results:

$130 \pm 3$ CPM/ppm of boron in aluminum

$169 \pm 4$ CPM/ppm of lithium in aluminum

## E. Interference From Other Ionizing Radiation

It is important to review the results of the experimental runs previously discussed and also a few special measurements made specifically to determine the effect and magnitude of the interference from the various unwanted radiations listed in Table II-3.

The fact that electrons are a prolific source of ionization in the detector is evidenced by the clutter on the oscilloscope sweeps. The rate at which they enter the chamber can be visualized by inspection of Figure 20b, which shows at least one medium or large pulse for every ten microseconds or so along the sweep, with no way of knowing how many smaller pulses are occurring coincidently with the larger ones. Interference from electrons would result when multiple coincidences create pulses large enough to pass the discriminator

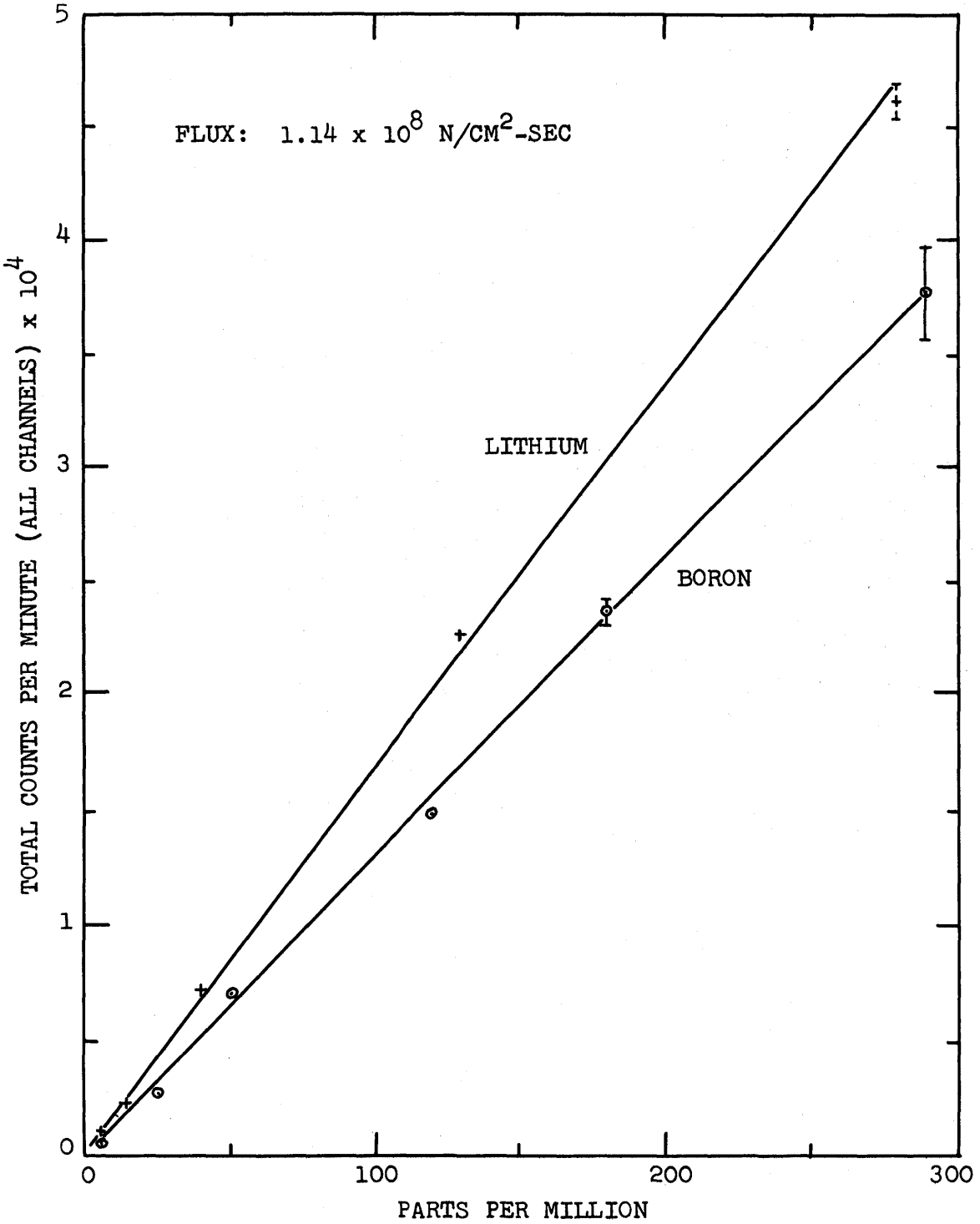


FIG. 26 PLOT OF MEASURED COUNT RATES FOR ALUMINUM STANDARDS CONTAINING KNOWN CONCENTRATIONS OF BORON OR LITHIUM (MAY 14 AND JUNE 6, 1963)

of the Model 132 Scaler or to be registered in the lowest sensitive channels of the TMC Analyzer. In the latter case, such pulses should be evidenced by high count rates in the lowest channels, but no indications of this situation were noted. If it did occur, it should be apparent in the curves of Figure 18, where the count rate due to boron and lithium is low and where operation in the innermost position would be most favorable for multiple pile-up of electron pulses.

In Figure 19, for the gold-lined cavity, the effect of space charge is most pronounced. The count rate indicates that the gold was relatively free of boron and lithium, as was expected, and so the ionization causing the space charge must have been due almost entirely to electrons. The cross section for the photoelectric interaction of gamma rays with electrons increases rapidly with the atomic number of the absorber, being proportional to the fourth or fifth power (depending upon the photon energy) of Z (19). Consequently, the electrons resulting from the photoelectric effect are in the range of 1,400-8,000 times as dense for the gold sample as for the aluminum samples. Although the energy spectrum for the gold is badly distorted, the ratio of total count rate at $1.71 \times 10^9$ neutrons/cm$^2$-sec. to count rate at $1.14 \times 10^8$ neutrons/cm$^2$-sec. and the ratio of the count rates for the lowest channels, where electron pulses would be recorded if there was much pile-up, are both equal to or less than 15, the ratio of the neutron fluxes. The opposite would be expected if electrons were not being effectively eliminated from the counting.

Beta rays from the decay of aluminum in the counter did not appear to contribute any detectable effects. As described in Subsection IV-C and illustrated in Figure 21, the build up of 2.3-minute aluminum-28 did not affect the energy spectrum of the 290 ppm boron standard. Based on the evidence of the two preceding paragraphs, pulse pile-up of light ionizing particles, including beta rays, does not contribute to the count rate even though serious distortion of the energy spectrum may occur.

An additional attempt was made to observe the effects of interfering radiations which are not the result of (n,α) reactions by reducing as much as practical the thermal neutron flux in the sensitive volume of the detector. This was accomplished by surrounding some of the samples, both aluminum and graphite, with 0.020" cadmium as described in Section III. The effect of this would be to reduce the counts from boron and lithium in the sample, in the structural materials, and in surface contamination. It would also reduce counts from fission fragments, and would reduce the number of decay betas from aluminum-28. However, it would not reduce the number of electrons, the alphas from the decay of naturally radioactive isotopes in the aluminum or graphite, or the recoils of nuclei struck by fast neutrons. It would in fact be expected to increase the first of these as the result of an increased number of capture gammas coming from the cadmium and also as the result of penetration of the 0.028" aluminum cavity wall by the photoelectrons generated in greater quantity (proportional to $Z^4$-$Z^5$) in the cadmium than they would be in aluminum. Electrons having energies greater than 0.5 Mev will penetrate the 0.028" aluminum.

The extent to which the (n,α) reactions were eliminated was measured by comparing the count rates for the 290 ppm boron and for the 280 ppm lithium with and without cadmium wrapping. The results, shown in Table IV-3, indicate that the wrapping was about 99% effective.

Table IV-3 also shows the reduction in count rates when the 99.9999% aluminum and the electrode-purity graphite are cadmium-wrapped. The reduction by only 95% may have been due to the fact that the shielding was less effective for these three samples, but the consistency of the results makes this quite unlikely. As will be seen later, the alphas from naturally radioactive isotopes are relatively unimportant, which leaves electrons and recoil nuclei as the only possible explanations for the fact that the count rates in these three samples were not also reduced by 99%.

TABLE IV-3

EFFECT OF CADMIUM SHIELD ON COUNT RATES

| Analysis (ppm) | Not Shielded Sample No. | CPM | Cd Covered Sample No. | CPM | % of Unshielded |
|---|---|---|---|---|---|
| 290 B | B-2a,b | $37,829 \pm 2,130$ | B-2c | $473 \pm 7$ | $1.25 \pm 0.07$ |
| 280 Li | Li-2a,b | $46,200 \pm 982$ | Li-2c | $417 \pm 6$ | $0.90 \pm 0.02$ |
| 99.9999% Al | S-a,b | $132 \pm 16$ | S-c | $7.4 \pm 0.2$ | $5.6 \pm 0.7$ |
| Graphite | Gr-c,d | $137 \pm 14$ | Gr-e,f | $5.7 \pm 0.3$ | $4.2 \pm 0.5$ |

Electrons do not appear to be a logical explanation in cases where the energy is not seriously distorted, as was pointed out earlier in this Subsection. Figure 27 shows the energy spectra for the boron and lithium with and without cadmium. The addition of cadmium changes the shape little, if any, although the electron flux in the chamber should be increased, as stated above. The increase, however, is not enough to distort the energy spectrum significantly and certainly not to the extent that it was distorted in Figure 18 and 19, for aluminum and gold. Electron pulse pile-up would be expected to contribute to the count rate only in the lowest channels. The energy spectra for the cadmium-wrapped aluminum and graphite samples (S-c and Gr-e), Figure 28 and Figure 29 show relatively high count rates in the lower channels, but the entire curves show count rates higher than 1% of the unshielded materials (S-a, S-b and Gr-c, Gr-d). (In Figure 29 the averages of five adjacent channels have been plotted for channels above No. 15 in order to reduce the scatter of the points.) Consequently, it is believed that electrons may be ruled out as contributing to the relatively high count rates of the 99.9999% aluminum and the electrode graphite samples with the cadmium shielding.

The effects of recoil nuclei were investigated briefly for hydrogen. The cadmium covered sample of 99.9999% aluminum

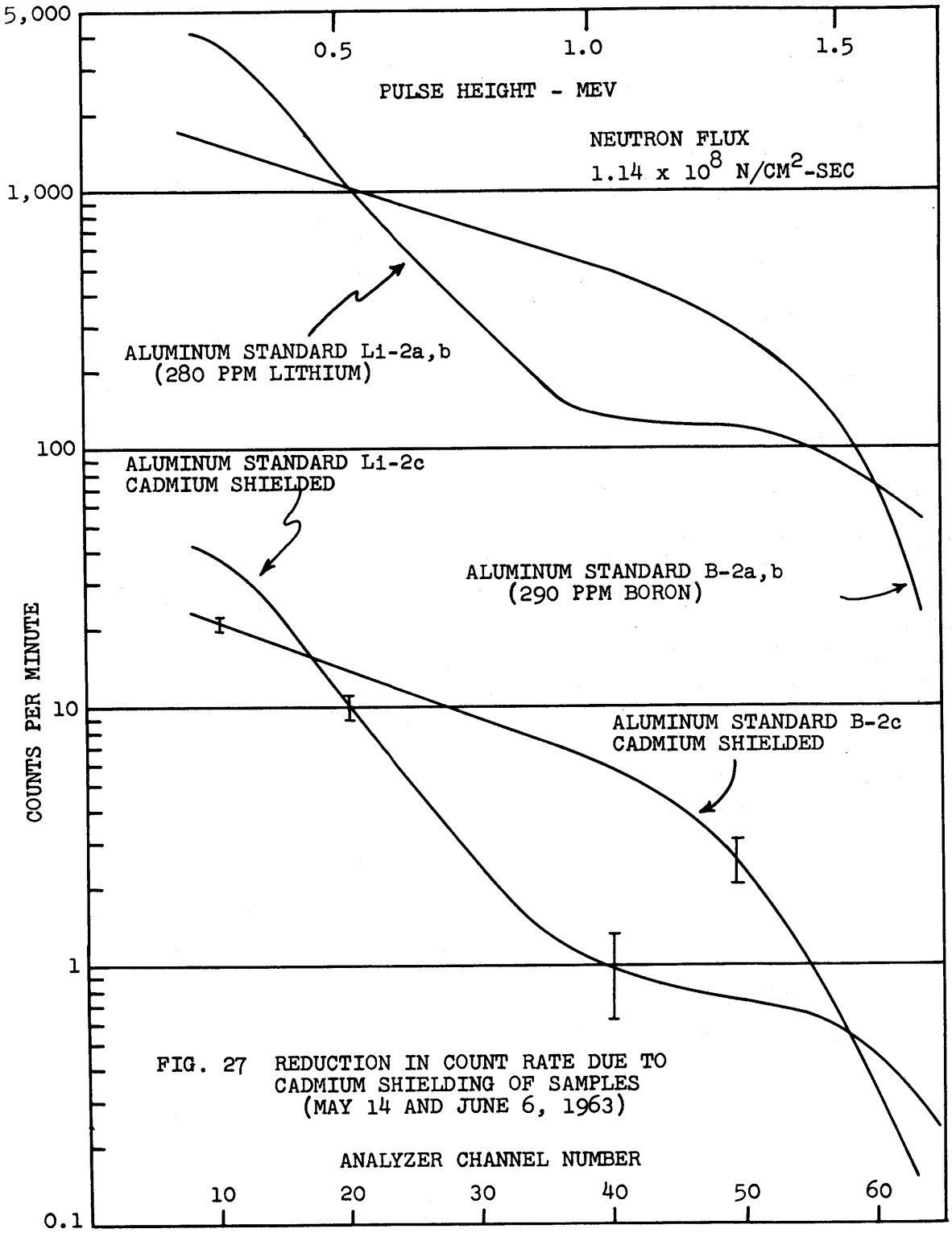


FIG. 27 REDUCTION IN COUNT RATE DUE TO CADMIUM SHIELDING OF SAMPLES (MAY 14 AND JUNE 6, 1963)

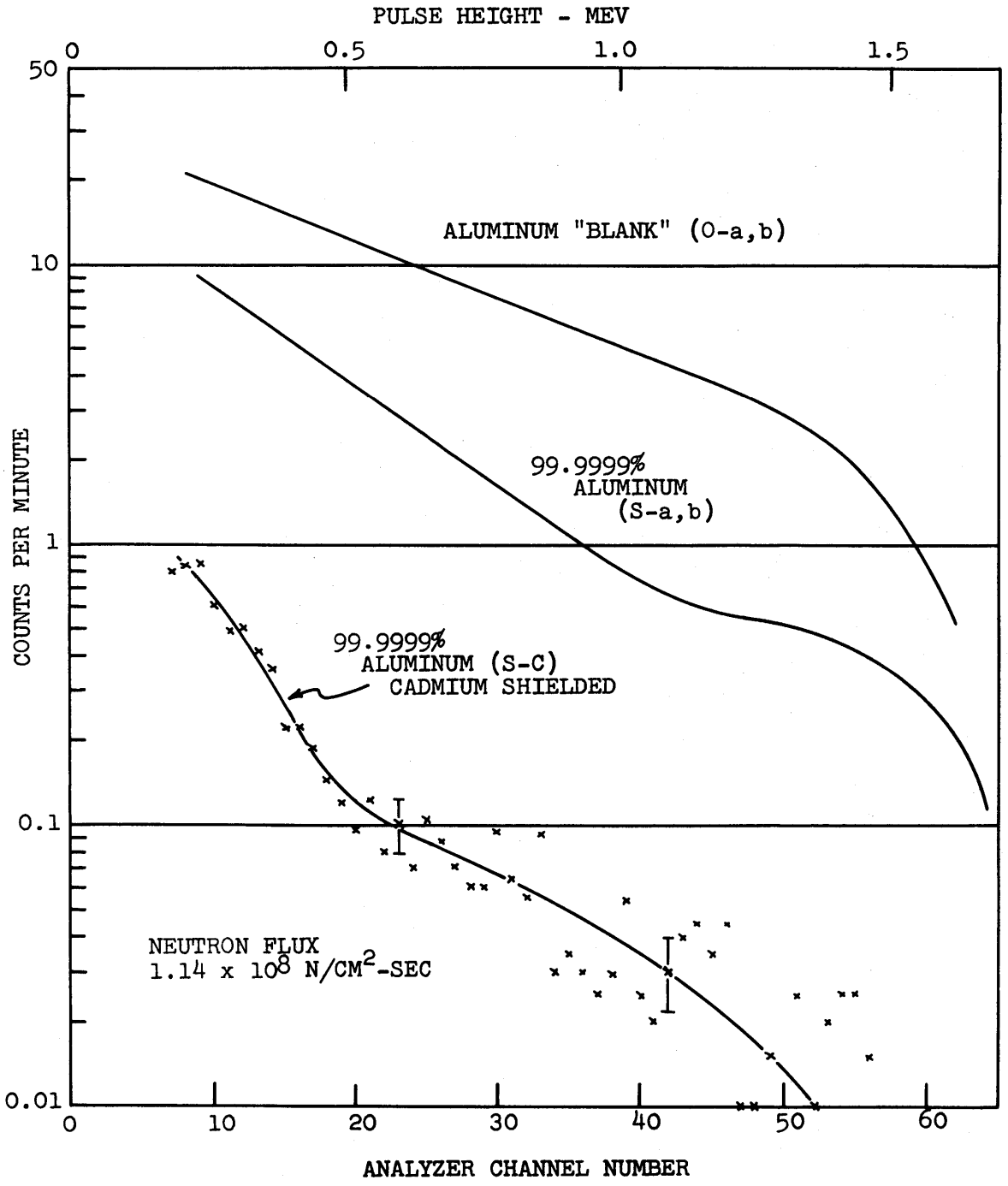


FIG. 28 ENERGY SPECTRA FOR HIGH PURITY ALUMINUM SAMPLES AND EFFECT OF CADMIUM SHIELDING ON ONE (MAY 14 AND JUNE 6, 1963)

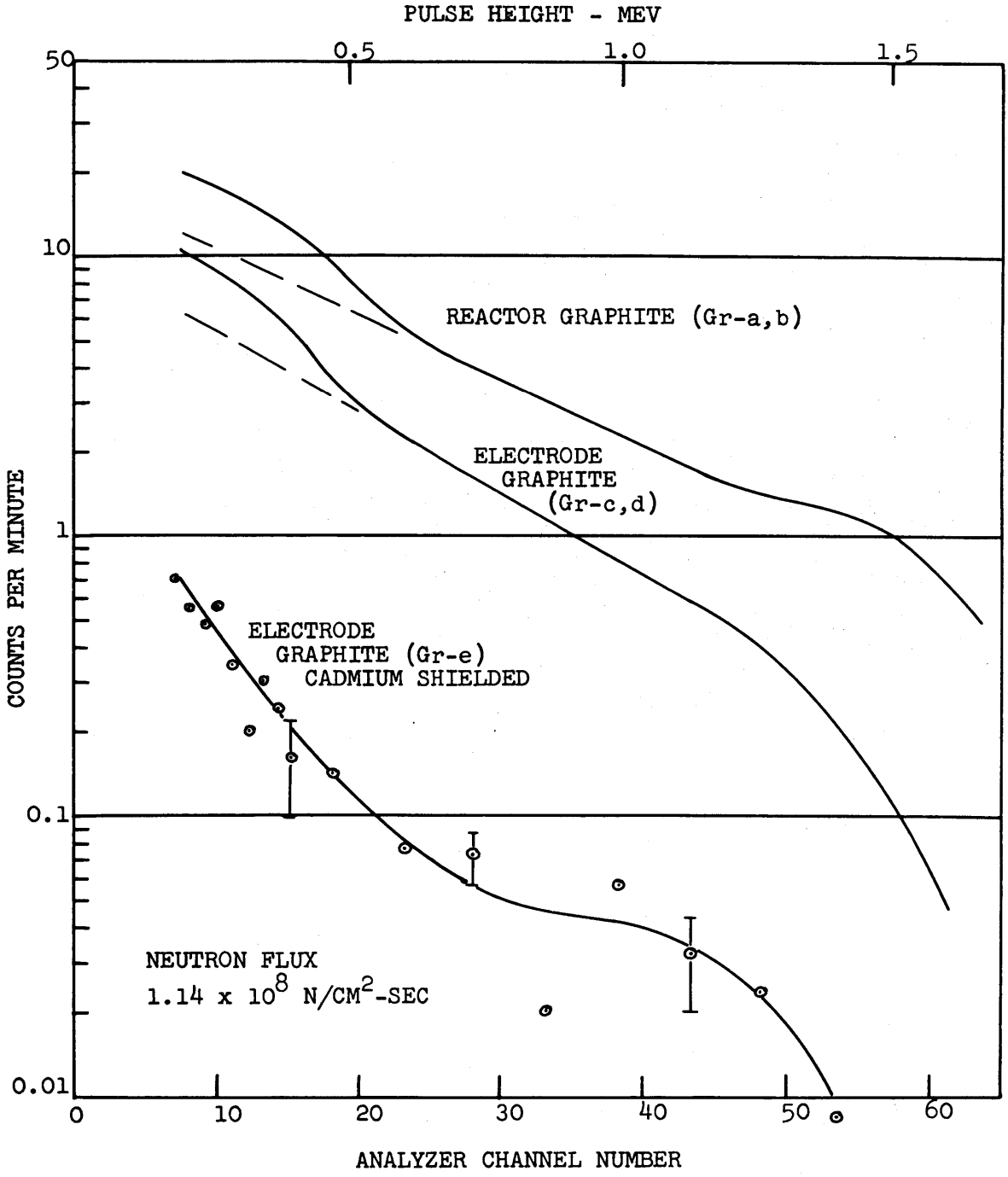


FIG. 29 ENERGY SPECTRA OF HIGH PURITY GRAPHITE SAMPLES AND EFFECT OF CADMIUM SHIELDING ON ONE (MAY 14 AND JUNE 6, 1963)

was counted both with 90% A-10% $Co_2$ and with 90% A-10% $CH_4$ for flux levels of $1.14 \times 10^8$ and $1.71 \times 10^9$ neutrons/$cm^2$-sec. At the lower flux, the run with each gas was 20 minutes long, and at the higher flux the runs were 10 minutes long. In each case, in order to eliminate possible variables, half the counting with A-$CO^2$ was carried out just before the A-$CH_4$ run, and the other half followed immediately afterwards. The results are tabulated below.

TABLE IV-4

EFFECT OF HYDROGEN IN COUNTER

| Neutron Flux ($n/cm^2$-sec.) | Gas | Count Rate (CPM) |
|---|---|---|
| $1.14 \times 10^8$ | A-$CO_2$ | $7.1 \pm 0.6$ |
| | A-$CH_4$ | $10.1 \pm 0.7$ |
| $1.71 \times 10^9$ | A-$CO_2$ | $34.9 \pm 1.9$ |
| | A-$CH_4$ | $59.2 \pm 2.4$ |

A significant increase in count rate with A-$CH_4$ is noted at both flux levels. The energy spectra are plotted in Figure 30 and show that the increase in rate is due to additional counts in the first few channels. Since only the gas was changed and since the counting characteristics of the gases were found to be very similar (Subsection IV-C), it is concluded that the replacement of oxygen by hydrogen in the counting gas was responsible for the increased count rate and the change in energy spectrum.

Except at the low energy end, the change in gas did not appear to change the spectrum. The low counts made an accurate comparison difficult; there was considerable scatter of the points even though the average of five adjacent channels was plotted, except for the first few channels where the count rate was higher. The effect of space charge at the higher flux was evident, however, the cadmium causing the high flux

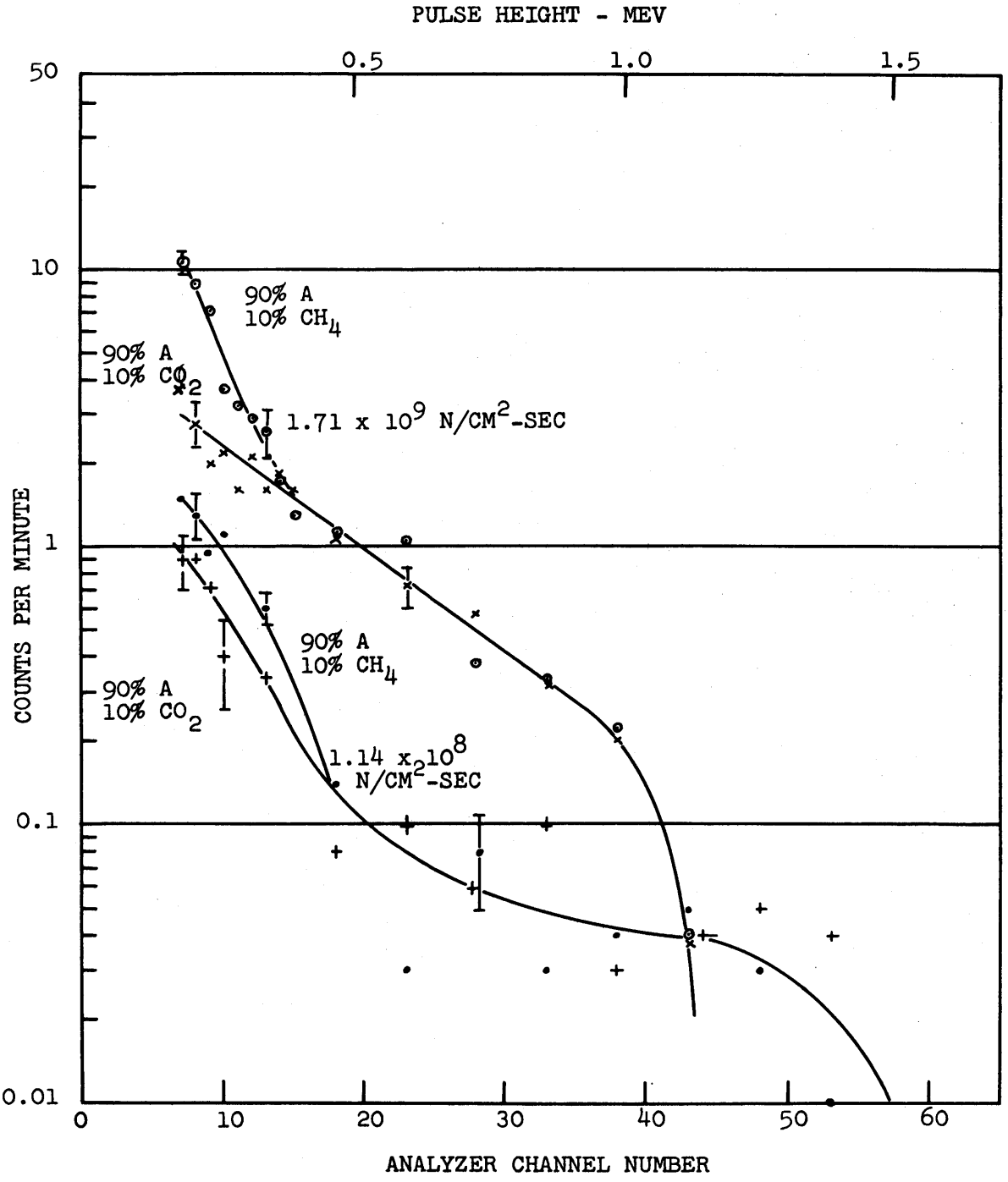


FIG. 30 EFFECT OF RECOIL PROTONS ON ENERGY SPECTRUM OF 99.9999% ALUMINUM SAMPLE, CADMIUM COVERED (JULY 11, 1963)

curve to drop to zero about 10 channel numbers before the low flux curve.

The graphite curves, Figure 29, show a departure at the low energy end, from the otherwise relatively straight plot up to about Channel No. 50. The possibility that this might be the result of recoil carbon nuclei or possibly pile-up of electron pulses was considered. In either case, the plot for the cadmium covered graphite should also show the effect, but much more prominently. At Channel No. 10, the unshielded electrode graphite (Gr-c, Gr-d) shows an increase of 3 to 4 CPM above what would be expected from a straight slope. If due to electron pulse pile-up or to recoil nuclei, this effect should also appear undiminished in the spectrum of the shielded sample. The count rate for the shielded sample, however, is only 0.5 CPM. The effect is probably due, therefore, to the manner in which the energy spectra of the individual $(n,\alpha)$ reaction products combine to form the total energy spectrum.

It would be of considerable interest to pursue further the question of the effects of fast flux, particularly in this region of the reactor, because this may be the factor which limits the sensitivity of the prompt activation analysis method for boron and lithium.

No attempts were made to determine the effects of boron or lithium which might be contained in the structural material. It is believed that $\alpha$, $H^3$, and $Li^7$ particles from these sources would enter the sensitive volume of the chamber only from the tungsten anode, the aluminum anode holder, the sulfur tip on the end of the anode, the aquadag coating on the tip, or the counting gas. The aluminum anode holder represents the largest area and could be fabricated in a future counter from a material like the 99.9999% aluminum (instead of type 6061, which probably would have a higher boron and lithium content). In addition, it could be made with a smaller surface area. However, it will be noted in Tables IV-1 and IV-2 that the count rates per part per million for the 5 ppm and 25 ppm boron standards and for the 15 ppm lithium standard were below the mean values of $130 \pm 3$ CPM/ppm for boron and $169 \pm 4$ CPM/ppm

for lithium. With the possible exception of the 5 ppm lithium standard, there does not appear to be any bias toward a higher count rate in the low concentration range covered by the standards, such as might be expected if the structural materials were contributing a constant amount to the observed count rates. For measurements at some lower concentration, however, such as 0.1 or 0.01 ppm, this could be a consideration.

Contamination of the sample surface was believed to be the cause of inconsistent results in several cases. Several standard samples were re-etched when they gave relatively high count rates. In all but one case, the 290 ppm boron standard (B-2b), a remeasurement then gave results which were consistent with other data. While surface contamination did not prove to be a major problem in the work with the standard samples, the results for the one case mentioned above indicate that it could cause difficulty even in the range of concentrations covered by the standards, and it undoubtedly would require further investigation if the sensitivity of the method were to be extended below the present range.

It was estimated in Table II-3 that the background count due to emission of alpha particles by naturally radioactive isotopes in the matrix materials would amount to a count rate on the order of 0.003 CPM/$cm^2$ of chamber surface, or about 0.01 CPM for this detector. Actual counting of alpha particles from six of the aluminum samples gave an average rate of 0.0017 $\pm$ 0.0003 CPM, well below the smallest count rates due to boron and lithium.

The background counting rate due to fission fragments from uranium-235 in the aluminum and in the graphite was measured for several samples, some of the runs being made at reduced anode voltages. At 1200 v. the $(n,\alpha)$ reaction products fell in Channels No. 6-17, with fission pulses spread from this point all the way to Channel No. 95. Figure 31 shows a comparison of the energy spectra for aluminum standard Li-1b (5 ppm lithium) made with operating voltages of 1400 volts and 1200 volts.

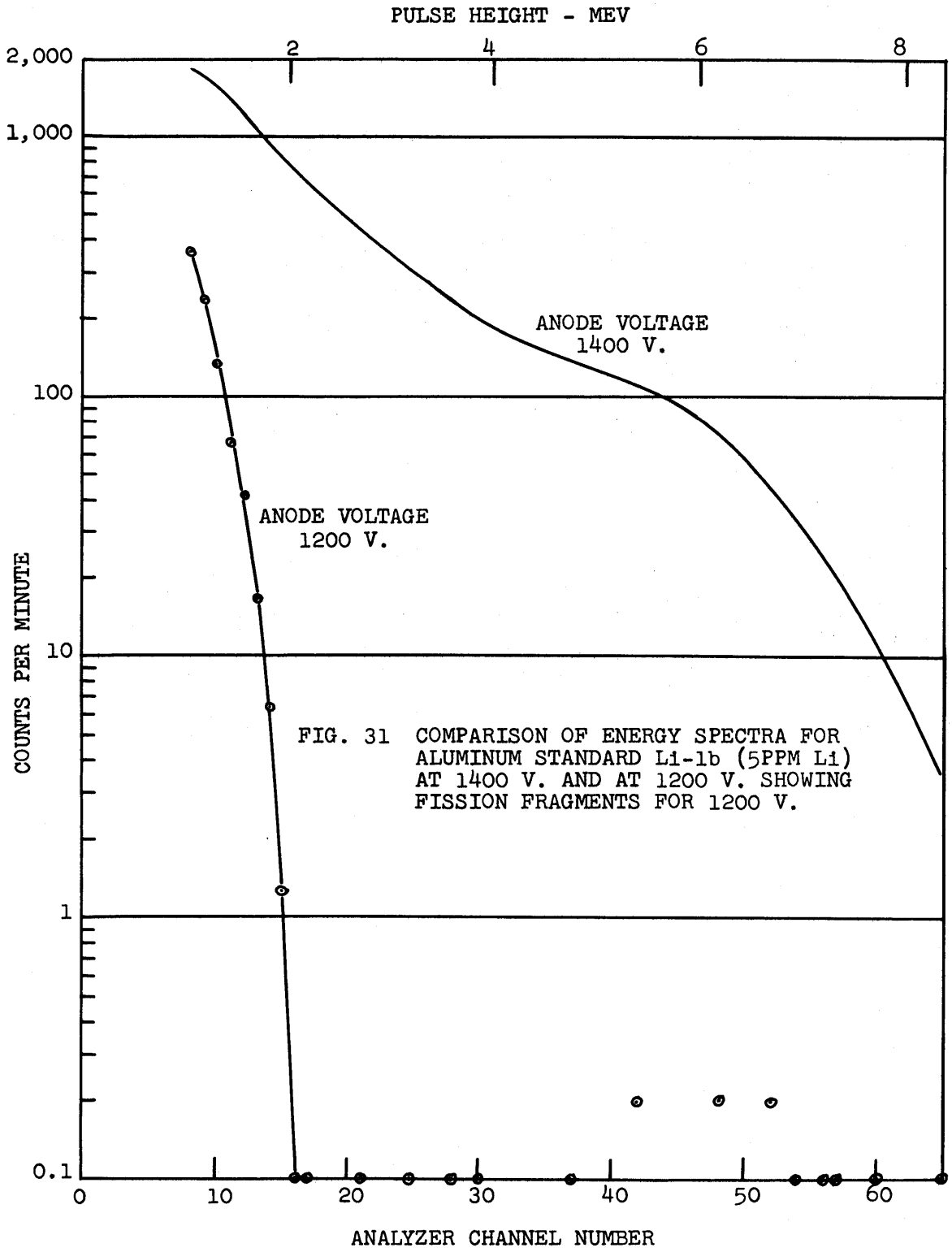


FIG. 31 COMPARISON OF ENERGY SPECTRA FOR ALUMINUM STANDARD Li-1b (5PPM Li) AT 1400 V. AND AT 1200 V. SHOWING FISSION FRAGMENTS FOR 1200 V.

Results for a few samples are listed below giving the fission count rate converted to a flux of $1.14 \times 10^8$ neutrons/$cm^2$-sec., for comparison with the (n,α) reaction products count rate, shown in the right hand column.

TABLE IV-5

SUMMARY OF FISSION FRAGMENT COUNT RATES

| Material | Sample No. | Fission Fragments (CPM) | α, $H^3$ and $Li^7$ (CPM) |
|---|---|---|---|
| Aluminum, 5 ppm Li | Li-1b | 0.23 ± 0.03 | 1,236 ± 98 |
| Aluminum "blank" | O-b | 0.09 ± 0.03 | 451 ± 31 |
| Aluminum, 99.9999% | S-b | 0.09 ± 0.03 | 133 ± 16 |
| Graphite, reactor | Gr-b | 0.07 ± 0.02 | 298 ± 25 |
| Graphite, electrode | Gr-d | 0.05 ± 0.01 | 137 ± 14 |

In all cases, the count rate due to fission fragments is well below 0.1% of the count rate due to boron and lithium, showing that this is not a source of interference in the measurements. If the sensitivity of the method were extended to the range of a few parts per billion, fission fragment counts might have to be taken into consideration. Even here they could be readily eliminated simply by using for the count rate an integrated count of the (n,α) reaction product spectrum, omitting the higher energy fission fragments, as was actually the case in most of the experimental runs where only one quarter of the TMC memory was utilized.

If an effective surface area of 3 $cm^2$ for the cavity is assumed, the 0.013 CPM/$cm^2$ at $10^8$ neutrons/$cm^2$-sec. estimated in Table II-3 converts to 0.04 CPM which is closely confirmed by the experimental results.

It is evident from the foregoing that this detector, in addition to its design purpose of measuring trace amounts of boron and lithium, is also capable of making much more sensitive and accurate measurements of trace quantities of

fissionable nuclides.

F. Activation Analysis of Unknown Samples

In the case of mixtures of boron and lithium in aluminum, it is possible to determine the concentration of each element by measuring first the slope of the energy spectrum in the region between 0.3 Mev and 0.9 Mev, approximately, which gives the ratio of boron to lithium, and second using the slope and the count rate in one of the channels to find the concentrations of each element.

General analytical expressions for this purpose are developed in the following manner.

Let $n_B$ = ppm boron

$n_{Li}$ = ppm lithium

$(C_B)_p$ = CPM for boron in Channel No. p, etc.

$(C_{B + Li})_p$ = CPM for mixture of boron and lithium in Channel No. p.

p = first channel number (lower) used to determine slope.

q = second channel number (upper) used to determine slope.

$(C_B/n_B)_p$ = CPM/ppm boron in Channel No. p, etc.

The logarithmic slope is given by:

$$\Delta \text{ ln/channel} = -\frac{1}{q-p}\left\{\ln\left[\left(\frac{C_B}{n_B}\right)_p n_B + \left(\frac{C_{Li}}{n_{Li}}\right)_p n_{Li}\right] - \ln\left[\left(\frac{C_B}{n_B}\right)_q n_B + \left(\frac{C_{Li}}{n_{Li}}\right)_q n_{Li}\right]\right\}$$

$$= -\frac{1}{q-p}\ln\frac{\left[\left(\frac{C_B}{n_B}\right)_p \frac{n_B}{n_{Li}} + \left(\frac{C_{Li}}{n_{Li}}\right)_p\right]}{\left[\left(\frac{C_B}{n_B}\right)_q \frac{n_B}{n_{Li}} + \left(\frac{C_{Li}}{n_{Li}}\right)_q\right]}$$

We can solve for the ratio $n_B/n_{Li}$, with the following result:

$$\frac{n_B}{n_{Li}} = - \frac{\left(\frac{C_{Li}}{n_{Li}}\right)_p - \left(\frac{C_{Li}}{n_{Li}}\right)_q e^{-(q-p)\Delta \ln/\text{chan.}}}{\left(\frac{C_B}{n_B}\right)_p - \left(\frac{C_B}{n_B}\right)_q e^{-(q-p)\Delta \ln/\text{chan.}}}$$

Substitution of the mean calibration values of CPM/ppm for this particular detector and use of the term $\Delta \ln$, or more specifically $\Delta \ln (C_{B + Li})$, which is equivalent to $-(q-p)\Delta \ln/$ channel (since $\Delta \ln$/channel always has a negative value), give the expression:

$$\frac{n_B}{n_{Li}} = - \frac{13.5 - 0.67\, e^{\Delta \ln (C_{B + Li})}}{5.1 - 2.03\, e^{\Delta \ln (C_{B + Li})}}$$

When an energy spectrum has been recorded (using the same experimental conditions), it is necessary only to subtract the natural log of the counts per minute in Channel No. 35 from the natural log of the counts per minute in Channel No. 10, ($\Delta \ln$), substitute in the above expression, and evaluate to get the ratio of boron to lithium in the sample, $(n_B/n_{Li})$.

The concentration of each element is obtained by use of the following balance:

$$(C_{B + Li})_p = \left(\frac{C_B}{n_B}\right)_p n_B + \left(\frac{C_{Li}}{n_{Li}}\right)_p n_{Li}$$

which is solved to get:

$$n_B = \frac{(C_{B + Li})_p}{\left(\frac{C_B}{n_B}\right)_p + \frac{1}{n_B/n_{Li}} \left(\frac{C_{Li}}{n_{Li}}\right)_p}$$

$$\text{and } N_{Li} = \frac{\left(C_{B + Li}\right)_p}{\frac{n_B}{n_{Li}}\left(\frac{C_B}{n_B}\right)_p + \left(\frac{C_{Li}}{n_{Li}}\right)_p}$$

Substitution of mean values gives:

$$n_B = \frac{\left(C_{B + Li}\right)_{10}}{5.1 + \frac{1}{n_B/n_{Li}}\,13.5}$$

$$n_{Li} = \frac{\left(C_{B + Li}\right)_{10}}{\frac{n_B}{n_{Li}}\,5.1 + 13.5}$$

The counts per minute recorded in Channel No. 10 and the previously determined ratio $n_B/n_{Li}$ are now substituted into the last two expressions to obtain the concentration of each element.

The analytical expressions may be employed, in slightly different form, to develop values for a table of slopes and count rates which may be used, with the same slope and count rate information for an unknown composition as is required for the analytical expressions, in order to determine the concentrations of boron and lithium in aluminum.

The results of measurements and tests to determine the effect and magnitude of the interference from undesired ionizing particles did not reveal any obstacles to using the described method of prompt activation analysis at concentrations somewhat below the lower limit of the range of standard aluminum samples studied. As mentioned in Section III, several types of high purity aluminum and graphite were obtained, and these were analyzed in the manner described above.

The samples tested were:

| Materials | Sample Code | Description |
|---|---|---|
| Aluminum | O-a, O-b | ALCOA "blank" |
| Aluminum | S-a, S-b | 99.9999% |
| Graphite | Gr-a, Gr-b | MIT Reactor graphite |
| Graphite | Gr-c, Gr-d | Spectroscopic electrodes |

The boron and lithium concentrations in the above samples were not available.

The energy spectrum for each of the samples was determined, the averages of the spectra having been given earlier in Figures 28 and 29. Use of the analytical expressions gives a boron to lithium ratio of 8.1. The other two expressions then give values of $2.9 \pm 1.0$ ppm boron and $0.4 \mp 0.4$ ppm lithium, with the errors coupled so that one value decreases when the other increases.

In a similar manner, the concentrations for the 99.9999% aluminum are found to be $0.4 \pm 0.3$ ppm boron and $0.5 \mp 0.2$ ppm lithium.

The analytical expressions cannot be used directly for determining the concentrations of boron and lithium in graphite, because the equipment was calibrated for tests on aluminum as the matrix. The counting efficiency will be different, and it might be that the slopes of the curves will not be quite the same for the same ratios of boron to lithium. The latter uncertainty can be resolved only by making measurements of the energy spectra on standard samples of graphite containing known boron or lithium concentrations.

An estimate can be made of the counting efficiency, however. Calculations taking into account the particle ranges in graphite and in aluminum show that counting rates for a given concentration of boron or lithium in the former are only 67% of the counting rates in the latter. The energy spectra for the graphite samples in Figure 29 leads then to an analysis

of 1.6 $\pm$ 1.2 ppm boron and 1.4 $\mp$ 0.5 ppm lithium for the reactor grade graphite (Gr-a, b) and to 0.5 $\pm$ 0.4 ppm boron and 0.8 $\mp$ 0.3 ppm lithium for the electrode graphite.

G. Limit of Sensitivity of the Present Counter

The various sources of interference which limit the sensitivity should be considered in the light of the determinations made on the several aluminum and graphite samples tested and of the low count rates achieved (without a determination of concentration) on the cadmium-wrapped samples. These results are summarized by Figure 32, a log-log plot of the above measurements. The two lines are drawn with slopes of 130 CPM/ppm for the boron and 169 CPM/ppm for the lithium. They are drawn solid in the range of the ALCOA aluminum standards, the results for which are plotted on the graph. Along the dashed portion of the line the results for the aluminum and graphite unknowns are plotted. The low count rates achieved by eliminating about 99% of the thermal neutrons are indicated by the arrows near the lower end of the dashed lines. In view of the fact that slopes for the energy spectra of these cadmium-wrapped samples were measurable, Figures 28 and 29, (although the accuracy of such a measurement is admittedly unknown), it may be anticipated that some kind of a determination could be made on aluminum or graphite which contained less than 0.1 ppm of boron and/or lithium, such an amount corresponding to the reduced count rates achieved by the cadmium shielding. If aluminum or graphite standards having known concentrations in the range of 0.1 - 0.001 ppm could be obtained, predictions of the sensitivity would be facilitated.

The limit of sensitivity of the present counter will depend upon the magnitude and frequency of ionizing events which occur in the counter in addition to the $\alpha$, $H^3$, and $Li^7$ particles from the boron and lithium to be measured. Electronic disturbances which give the appearance of heavy ionizing particles should also be taken into account.

The ionizing radiations summarized in Tables II-1 and II-3 are listed again below for the purpose of consolidating the experimental data relating to each item. The count rates

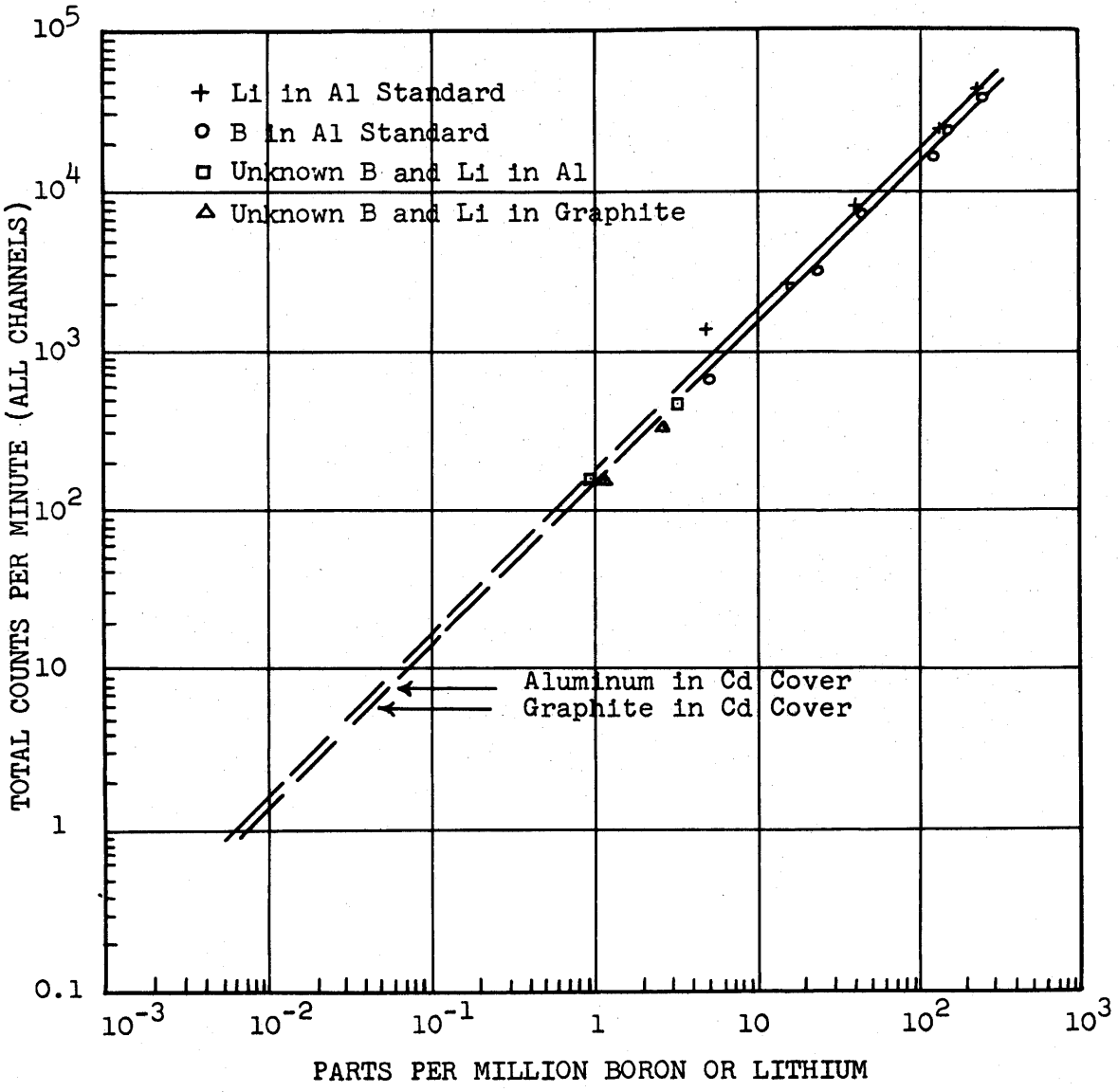


FIG. 32 LOG-LOG PLOT OF STANDARD AND UNKNOWN SAMPLES (MAY 14 AND JUNE 6, 1963)

given are for the counter and samples used (effective area of chamber about 3 $cm^2$) and for the neutron flux in the usual operating position of the pile oscillator tube in port 12CH1, measured at 1.14 x $10^8$ neutrons/$cm^2$-sec.

TABLE IV - 6

SUMMARY OF COUNT RATES MEASURED IN DETECTOR

| Items | Particle | Source | Count Rate |
|---|---|---|---|
| 1. | $\alpha$ | B to be assayed | 130 $\pm$ 3 CPM/ppm |
| 2. | $Li^7$ | | |
| 3. | $\alpha$ | Li to be assayed | 169 $\pm$ 4 CPM/ppm |
| 4. | $H^3$ | | |
| 5. | $e^-$ | Gammas | Zero |
| 6. | $\beta$ | Al decay | Zero |
| 7. | $\alpha$, $Li^7$, $H^3$ | B and Li in structural materials | Not determined |
| 8. | $\alpha$ | $U^{238}$, etc. | 0.01 CMP max. |
| 9. | f.f. | $U^{235}$ (n,f) | 0.23 CPM max. |
| 10. | recoil nuclei | Fast neutrons | 6 CPM max. |
| 11. | a, $Li^7$, $H^3$ | Surface contamination | Not determined |
| 12. | - | Electronic noise | 0.20 CPM max. |

It appears that the count rates due to interfering radiations which were measured as part of this investigation were at most 4% of the count rates for boron and lithium at a concentration of one part per million.

It is believed that this percentage, for the items measured, can be made much smaller. The electronic noise, at 0.20 CPM maximum, gave an average count rate of 0.09 CPM, and the fact that there were extended periods of much quieter operation would indicate that this source of interference could probably be rendered negligible in comparison to other causes of counts.

The fission fragment background can be almost completely eliminated by counting only pulses having energies of 2 Mev

and below, excluding the high energy fission pulses.

It is difficult, however, to estimate the sensitivity of this analytical method without further information on the effects of Items No. 7, 10, and 11. No constant component, such as would be expected if Item No. 7 were important, was noted in the counting rates at concentrations down to 5 ppm. If present, such an effect would not be expected to become dominant for at least another factor of ten, at which point, if necessary, greater care in the selection and preparation of anode materials should improve the sensitivity still further.

The extent to which surface contamination of the samples interfered with the accuracy of the determinations is not known. It apparently occurred and was corrected with little effort in several cases, but not in another. The irregularities in some of the low count rate curves, such as the 99.9999% aluminum in Figure 18, particularly at the higher flux, suggest possible surface contamination with boron or lithium. However, there seems to be no reason why, with the focusing of some attention on this problem, it should become a serious limitation on the sensitivity of the method for at least another factor of ten or one hundred below one part per million.

The effect of fast neutrons was investigated directly only with respect to hydrogen. The introduction of a very small amount of this element as part of the counting gas caused an increase in the count rate of 3 CPM. Due to the fact that there are comparatively large quantities of aluminum or graphite surrounding the chamber, when these materials are being tested, it is not clear how the count rate is affected by the recoil nuclei of such atoms struck by fast neutrons. If there is such an effect on these moderately heavy nuclei, it very likely would be the result of first collisions by fission neutrons (or at least fission neutrons which have suffered only a glancing collision and hence lost little of their original energy). The number of these striking the counter could be appreciably reduced if it were possible

to locate the counter at some position in the heavy water exponential tank, or perhaps in the pedestal under the tank, so that fission neutrons would have to make at least one large-angle collision before reaching the counter.

It is primarily the uncertainty in estimating the effects of fast neutrons and the further uncertainty regarding the possibility of improving the situation (if it should prove to be a limiting factor) that make it difficult to estimate the potential sensitivity of this prompt activation analysis method. If we assume that the effect has a magnitude of the same order as the effect on hydrogen (3 CPM), or that most of the counts for the high-purity aluminum and graphite with cadmium covers (perhaps 80% of 7.4 CPM and 5.4 CPM, Table IV-3) are due to fast neutrons, then the sensitivity would be limited to the region of 0.1 ppm and would depend on how accurately the slope of the energy spectrum could be determined in the presence of the recoil nuclei.

In a flux of $1.14 \times 10^8$ neutrons/$cm^2$-sec., 2% accuracy in the total count rate for concentrations of one part per million can be obtained in just under 20 minutes of counting, and it is possible to make a reasonable measurement of the slope of the energy spectrum. If the possible sources of interference can be controlled, a reduction in concentration to 0.1 ppm or 0.01 ppm can be gained by extending the counting time a corresponding amount (or by accepting less accuracy with shorter counting times).

An increase in flux level will, of course, increase the count rates. However, it will be recalled that distortion of the energy spectrum, which affects slope measurements, began to take place at fluxes above $10^8$ neutrons/$cm^2$-sec. for aluminum. For materials of higher atomic number, the increased electron flux and consequent space charge might force the use of a flux level below $10^8$ neutrons/$cm^2$-sec.

# SECTION VI

# APPENDICES

## APPENDIX A - TABLE A-1

## POSSIBLE NEUTRON-GAMMA REACTIONS FOR LIGHT ELEMENTS (3)

| Element | Reaction | Natural Abundance of Reactant | Thermal Neutron Cross Section (barns) | Half-life of Product | Mode of Decay (Energy in Mev) |
|---|---|---|---|---|---|
| H | $H^1(n,\gamma)H^2$ | 99.985% | 0.330 | stable | - |
| | $H^2(n,\gamma)H^3$ | 0.015% | $0.57(10^{-3})$ | 12.26 yr. | $\beta^-(0.018)$ |
| He | $He^3(n,\gamma)He^4$ | $1.3(10^{-4})$% | n.r. * | stable | - |
| | $He^4(n,\gamma)He^5$ | 100% | 0 | - | - |
| Li | $Li^6(n,\gamma)Li^7$ | 7.5% | n.r. | stable | - |
| | $Li^7(n,\gamma)Li^8$ | 92.5% | 0.033 | 0.86 sec. | $\beta^-$(13-90%, + others) $\gamma$ n.r. |
| Be | $Be^9(n,\gamma)Be^{10}$ | 100% | 0.01 | $2.5(10^6)$yr. | $\beta$(0.557) |
| B | $B^{10}(n,\gamma)B^{11}$ | 18.7% | n.r. | stable | - |
| | $B^{11}(n,\gamma)B^{12}$ | 81.3% | <0.05 | 0.022 sec. | $\beta^-$(13.4-98% + others) $\gamma$(4.43-1.7%) |
| C | $C^{12}(n,\gamma)C^{13}$ | 98.89% | 0.0033 | stable | - |
| | $C^{13}(n,\gamma)C^{14}$ | 1.11% | 0.0007 | $5.6(10^3)$yr. | $\beta^-(0.156)$ |
| N | $N^{14}(n,\gamma)N^{15}$ | 99.635% | 0.10 | stable | - |
| | $N^{15}(n,\gamma)N^{16}$ | 0.365% | $0.024(10^{-3})$ | 7.36 sec. | $\beta^-$(several) $\gamma$(6.13,7.10) |
| O | $O^{16}(n,\gamma)O^{17}$ | 99.759% | n.r. | stable | - |
| | $O^{17}(n,\gamma)O^{18}$ | 0.037% | n.r. | stable | - |
| | $O^{18}(n,\gamma)O^{19}$ | 0.204% | $0.21(10^{-3})$ | 29.4 sec. | $\beta^-$(2.9-70%, 4.5-30%) $\gamma$(several) |

* not reported

## APPENDIX B - TABLE B-1

SUMMARY OF (n,p) AND (n,α) REACTIONS FOR WHICH THERMAL CROSS SECTIONS ARE GIVEN (3)

| Element | Reaction | Natural Abundance of Reactant | Thermal Neutron Cross Section (barns) | Half-life of Product | Mode of Decay (Energy in Mev) |
|---|---|---|---|---|---|
| He | $He^3(n,p)H^3$ | $1.3(10^{-4})\%$ | $5.4(10^3)$ | 12.26 yr. | $\beta^-(0.018)$ |
| Li | $Li^6(n,\alpha)H^3$ | 7.5% | 945 | 12.26 yr. | $\beta^-(0.018)$ |
| B | $B^{10}(n,\alpha)Li^7$ | 18.7% | $4(10^3)$ | stable | - |
| | $B^{10}(n,p)Be^{10}$ | 18.7 | $< 0.2$ | $2.5(10^6)$ yr. | $\beta^-(0.557)$ |
| N | $N^{14}(n,p)C^{14}$ | 99.635% | 1.76 | $5.6(10^3)$yr. | $\beta^-(0.156)$ |
| O | $O^{17}(n,\alpha)C^{14}$ | 0.037% | 0.5 | $5.6(10^3)$yr. | $\beta^-(0.156)$ |

# APPENDIX C

## BIBLIOGRAPHY


1. Leddicotte, G. W., Mullins, W. T., Bate, L. C., Emery, J. F., Druschel, R. E., and Brooksbank, W. A., Jr., "The Use of Neutron Activation Analysis in Analytical Chemistry," Progress in Nuclear Energy, Series IX, Analytical Chemistry, Vol. 1, Pergamon Press, 1959.

2. Koch, R. C., Activation Analysis Handbook, Air Force Cambridge Research Center Report No. AFCRC-TR-59-139 (1958).

3. Sullivan, W. H., Trilinear Chart of Nuclides, U. S. Government Printing Office, Washington, D. C., 1957.

4. Mayr, G., "Activation Analysis with Nuclear Emulsions," Nucleonics 12, No. 5, 58 (1954).

5. Mayr, G., Brunner, H. D., and Brucer, M., "Boron Detection in Tissues Using the (n,α) Reaction," Nucleonics 11, No. 10, 21 (1953).

6. Wanke, H., and Monse, E. U., "Scintillation Counting of (n,α) or (n,f) Reaction for the Isotopic Analysis of Lithium, Boron, and Uranium," Z. Naturforsch. 10a, 667 (1955) (In German).

7. Fiti, M., Mantescu, C., and Costea, T., "Determination of Boron in Minerals by the Detection of α-particles from the Reaction $B^{10}$ (n,α)$Li^{7}$," Academia Republicii Populare Romine, Institutul de Fizica Atomica Si Institutal de Fizica, Studii Si Cercetari de Fizica, 11 423-30 (1960) (In Rumanian).

8. Kienberger, C. A., Greene, R. E., and Voss, F. S., "Determination of $Li^{6}$ by Fission Counting," USAEC Report No. K-1042 (1963).

9. Gill, R. A., "Proton Activation Analysis in Determination of Submicrogram Amounts of Boron in Silicon," AERE C/R 2758 (1958).

10. Davis, H. M., Milner, G. W. C., Garton, F. J. W., Shalgosky, H. I., and Jenkins, E. N., "Recent Developments in Analysis with Special Reference to Reactor Research," Progress in Nuclear Energy, Series IX, Analytical Chemistry, Vol. 1, Pergamon Press, 1959.

11. Lipis, L. V., "Spectral Analysis of Pure Materials," Soviet Physics Uspekhi, Vol. 2 (68) No. 3, 393-9 (1959).

12. Price, W. J., Nuclear Radiation Detection, McGraw-Hill Book Company, Inc., New York, 1958.

13. Everling, F., Koenig, L. A. Mattauch, J. H. E., and Wapstra, A. H., 1960 Nuclear Data Tables, Part 1, Consistent Set of Energies Liberated in Nuclear Reactions, National Academy of Sciences, National Research Council, Washington, D. C., 1961.

14. "Nuclear Data Group, Nuclear Data Sheets," Vol. 5, Section 1, September, 1962, National Academy of Sciences, National Research Council.

15. Rossi, B. B., and Staub, H. H., Ionization Chambers and Counters, McGraw-Hill Book Company, Inc., New York, 1949.

16. Madell, John T., "Spatial Distribution of the Neutron Flux on the Surfaces of a Graphite-Lined Cavity," Sc.D. Thesis, Department of Nuclear Engineering, M. I. T., Cambridge, Mass. (1961).

17. Bratton, J. K., "A Pile Oscillator for Measurement of Neutron Cross Sections in the M. I. T. Reactor," M.S. Thesis, Department of Nuclear Engineering, M. I. T., Cambridge, Mass. (1959).

18. Reilly, W. F., "Construction and Calibration of a Standard Pile," M.S. Thesis, Department of Nuclear Engineering, M. I. T., Cambridge, Mass. (1958).

19. Evans, R. D., The Atomic Nucleus, McGraw-Hill Book Company, Inc., New York, 1955.